Published for SISSA by Springer

Received: October 17, 2023
Revised: February 28, 2024
Accepted: March 20, 2024
Published: April 18, 2024

ALP-assisted strong first-order electroweak phase transition and baryogenesis

Keisuke Harigaya[a,b,c] **and Isaac R. Wang**[d]

[a] *Department of Physics, University of Chicago, Chicago, IL 60637, U.S.A.*
[b] *Enrico Fermi Institute and Kavli Institute for Cosmological Physics, University of Chicago, Chicago, IL 60637, U.S.A.*
[c] *Kavli Institute for the Physics and Mathematics of the Universe (WPI), The University of Tokyo Institutes for Advanced Study, The University of Tokyo, Kashiwa, Chiba 277-8583, Japan*
[d] *New High Energy Theory Center, Department of Physics and Astronomy, Rutgers University, Piscataway, NJ 08854, U.S.A.*

E-mail: kharigaya@uchicago.edu, isaac.wang@rutgers.edu

Abstract: Axion-like particles (ALPs) can be naturally lighter than the electroweak scale. We consider an ALP that couples to the Standard Model Higgs to achieve the strong first-order electroweak phase transition. We discuss the two-field dynamics of the phase transition and the associated computation in detail and identify the viable parameter space. The ALP mass can be from the MeV to GeV scale. Baryon asymmetry can be explained by local baryogenesis without violating the current electron and atom electric dipole moment bound in most of the viable parameter space. The viable parameter space can be probed through Higgs exotic decay, rare kaon decay, the electron and atomic electric dipole moment, and the effective number of neutrinos in the cosmic microwave background in the future. The gravitational-wave signal is too weak to be detected.

Keywords: Axions and ALPs, Baryo-and Leptogenesis, Phase Transitions in the Early Universe

ArXiv ePrint: 2309.00587

Open Access, © The Authors.
Article funded by SCOAP[3].

https://doi.org/10.1007/JHEP04(2024)108

JHEP04(2024)108

Contents

1 Introduction **1**

2 The model **4**
- 2.1 The tree-level potential 4
- 2.2 One-loop corrections 7

3 The electroweak phase transition **9**
- 3.1 Finite temperature corrections 9
- 3.2 Phase transition and bubble nucleation 11
- 3.3 Enhancement of the phase transition 14

4 Local electroweak baryogenesis **14**

5 UV completion **16**
- 5.1 Composite UV completion 17
- 5.2 Perturbative UV completion 19

6 Experimental signals **19**
- 6.1 Higgs exotic decay 19
- 6.2 Scalar direct production 20
- 6.3 Rare meson decay 20
- 6.4 Heavy particles at colliders 21
- 6.5 Electron electric dipole moment 21
- 6.6 Atomic electric dipole moment 23
- 6.7 Effective neutrino number 23

7 Conclusion and discussion **24**

A Phase transition strength in SM with lighter Higgs mass and computational uncertainties **25**

1 Introduction

The predominance of matter over antimatter in the universe is a well-established fact. However, despite the success of the Standard Model (SM) of particle physics, the origin of matter-antimatter asymmetry, referred to as baryogenesis, is still obscure. As pointed out by Sakharov, successful baryogenesis mechanisms must contain baryon number (B) violation, C and CP violation, and out-of-thermal-equilibrium processes [1]. Since the first proposal in 1985 [2], electroweak baryogenesis (EWBG) has drawn significant attention. Indeed, the baryon symmetry is anomalous at the quantum level in the SM and is violated by the weak sphaleron process [2–6]. Moreover, a CP-violating phase exists in the CKM matrix of the

JHEP04(2024)108

weak sector [7, 8]. If the electroweak phase transition (EWPT) is a strong first-order phase transition (SFOPT), the out-of-equilibrium condition will also be satisfied. Nevertheless, the SM EWPT has been shown to be a smooth crossover that cannot satisfy the out-of-equilibrium condition [9–20]. Furthermore, even if the phase transition is a SFOPT, the resulting baryon asymmetry from the EWBG in the minimal SM has been found to be much smaller than the observed value due to the tiny Yukawa couplings of quarks and the CKM mixing [21–25]. Therefore, new physics is necessary in order to enhance the strength of the EWPT and provide additional CP-violation. One way to enhance the strength of the phase transition is to extend the SM scalar sector with an extra singlet scalar that generates trilinear terms at tree level [26–50]. Such trilinear terms generate a barrier at finite temperature between the true vacuum and the false vacuum during the phase transition and thus can enhance the strength of the EWPT. These models often predict signals of extra scalar production, Higgs exotic decay, and gravitational waves (GWs). Moreover, additional CP-violation may exist in the scalar sector, which typically can be observed in future electron electric dipole moment (EDM) measurements.

To affect the EWPT, the scalar particle must be lighter or at most around the electroweak scale. This leads to a question concerning naturalness akin to that of Higgs: why can this singlet have a mass much smaller than other fundamental scales? In addition, in light of the current extensive and comprehensive experimental search for dark-scalar mixing with the Higgs, the scalars are required to be weakly interacting with the Higgs, and, naturally, with other SM particles. These two hints motivate considering scalar particles that are naturally light and weakly interacting.

One well-known example of this type of particles is the axion-like particle (ALP). The ALP is the angular degree of freedom of a complex scalar $P = |P| \exp(iS/f)$ with rotational U(1) symmetry. This symmetry is spontaneously broken at the energy scale f, leaving S as the remaining singlet scalar particle at the EW scale (or below), with a shift symmetry $S \to S + \delta S$. The shift symmetry can be explicitly broken to give a potential of S and coupling with the Higgs. The fact that the ALP is the pseudo-Nambu-Goldstone boson (pNGB) makes it naturally light and weakly interacting.

The potential of S and its leading order coupling with the Higgs is [51]

$$V(H,S) = -(\mu_H^2 - Af\cos\delta)|H|^2 + \lambda|H|^4 + \mu_S^2 f^2\left(1-\cos\left(\frac{S}{f}\right)\right) - Af\left(|H|^2 - v^2\right)\cos\left(\frac{S}{f}-\delta\right), \tag{1.1}$$

where $v \simeq 174\,\text{GeV}$ is the measured EW vacuum expectation value (vev) of the Higgs field. Here we choose the minima of S after the EWPT to be $S = 0 + 2n\pi$ by the shift of S. There is a phase difference δ between the potential of S and the interaction term with the Higgs. This phase can arise from CP-violation in the UV completion of the model.

In large f limit, the potential becomes

$$V(H,S) = -\mu_H^2|H|^2 + \lambda|H|^4 + \frac{1}{2}\mu_S^2 S^2 - A'S(|H|^2 - v^2), \tag{1.2}$$

where $A' \equiv A\sin\delta$. This potential was first introduced in [34] and reviewed in [37]. The naturalness of the lightness of S is pointed out in [52], with a thorough investigation of the

JHEP04(2024)108

two-field dynamics of the phase transition, vacuum metastability, and MeV scale parameter space. We call the model with the potential in eq. (1.2) "the simplified model" throughout this paper. This potential, along the path $S(H)$ where $\partial V/\partial S = 0$, becomes

$$V(H, S(H)) = -\frac{1}{2}\mu_H^2 h^2 + \frac{1}{4}\left(\lambda - \frac{A'^2}{2\mu_S^2}\right) h^4. \tag{1.3}$$

The effective quartic coupling, $\lambda - A'^2/(2\mu_S^2)$, becomes small and this is often presumed to make the EWPT strongly first-order because the thermal effect becomes more important in comparison with the zero-temperature potential. Here the strong first-order EWPT is usually defined to be $v_c/T_c \geq 1$, where T_c denotes the critical temperature of the phase transition and v_c is the Higgs vev at T_c.

This conclusion holds true if the finite-temperature effective potential is computed under high-temperature expansion without proper resummation and one-loop zero-temperature correction (for example, see [53].) Such a computation technique is also used in previous works for the simplified model [34, 37, 52]. However, in the SM with a small quartic coupling (i.e., a small Higgs mass), once thermal resummation and the Coleman-Weinberg correction are properly included, the EWPT is significantly weakened and is not strong enough [54] (see [55] for a recent review.). The main suppression comes from the top quark Yukawa. We performed a two-loop computation with the state-of-the-art dimensional reduction method with the help of the `DRalgo` package [56] to check the viability of the simplified model. (See [57–60] for the original references of dimensional reduction and [61–64] for recent applications and reviews.) We find that the EWPT is not strong enough to prevent the washout of baryon number for the simplified model [34, 37, 52], see appendix A, where we show the numerical results of various computation methods and comment on the uncertainties. Although higher-order computations and/or more careful treatment on various sources of uncertainties may finally reveal that the simplified model can work, the viability of the simplified model is questionable.[1]

In this work, we consider the full potential of an ALP in eq. (1.1), emphasizing the deviation from the simplified model as f gets smaller. With a smaller UV scale f, the higher-order terms in S may be effective and enhance the EWPT. This work focuses on this full potential, with the thermal effective potential computed at one-loop level with proper resummation and zero-temperature corrections. We show that the full ALP+SM model does give an SFOPT in a wide range of the parameter space. This enhancement does not require a large mixing angle between the ALP and Higgs, and the model works even for a MeV scale ALP, and thus opens a window for a SFOPT by extra scalars.

In addition to the enhancement of the phase transition strength, this model provides chances to produce the observed amount of baryon asymmetry in the universe (BAU) via the local electroweak baryogenesis mechanism [65–67]. Traditional local electroweak baryogenesis considers an effective operator $|H|^2 W\tilde{W}/M^2$, where M is some UV scale, to produce a baryon number asymmetry proportional to $(\Delta h/M)^2$. Since δh is around the weak scale, to explain

[1] Previous lattice simulations claiming an SFOPT with a small Higgs mass $m_H \simeq 35\,\text{GeV}$ in the SM were based on pure SU(2) + Higgs theory, and thus the negative contribution from top Yukawa was not included. For example, see ref. [9, 11, 12, 14, 20]. Those full SM simulations with a proper top quark mass considered only reached a physical Higgs mass $m_H \simeq 50\,\text{GeV}$, corresponding to $v_c/T_c \simeq 0.7$, which is consistent with the two-loop computation of ref. [54].

JHEP04(2024)108

the observed BAU requires the UV scale M not much above the weak scale, which leads to a too large electron EDM. The mechanism was ruled out shortly after its proposal. In the model we consider, on the other hand, we may consider the dimension-5 couplings of the ALP with the W boson or the SU(2) charged fermions suppressed by a UV scale M. Because the shift of S during the phase transition is much above the weak scale, the UV scale M may be much above the weak scale, so the EDM constraint is avoided in most of the viable parameter spaces.

We discuss various ways to probe this ALP model. Unfortunately, we find that the gravitational-wave signal from the EWPT is too weak to be detected. But scalar direct production can put a stringent constraint on the GeV scale ALP, which can be probed in the future by Higgs exotic decay. The MeV scale ALP can be probed by beam-dump experiments searching for rare Kaon decays, such as NA62 or KLEVER. Furthermore, the MeV scale ALP contributes negatively to the effective neutrino numbers of the universe, which can be probed by the future Cosmic Microwave Background (CMB)-S4 experiment.

The coupling of the Higgs with a NGB to affect the EWPT was discussed in the literature [51, 68–71]. In [68, 70, 71], the Higgs is a composite field to solve the electroweak hierarchy problem and is also a NGB. In this paper, we consider the case where the Higgs is a fundamental scalar field and do not address the electroweak hierarchy problem by the compositeness of the Higgs. The smallness of the electroweak scale may be explained by anthropic requirements [72–74] or (partially) by supersymmetry [75–78]. Refs. [51, 69] consider the same IR model in eq. (1.2) as well as local baryogenesis by the coupling of S with the $\mathrm{SU}(2)_L$ gauge bosons. We include one-loop corrections to the zero-temperature potential as well as resummation in the computation of the thermal potential, which can significantly suppress the strength of the PT as described above. The one-loop corrections to the zero-temperature potential can also destabilize the electroweak vacuum, but we will show that the lifetime of the vacuum is still long enough. We also present different UV completions from refs. [51, 69].

This paper is organized as follows. In section 2, we discuss the basic settings of the model as well as the loop corrections. Naturalness requirement and metastability are also discussed in this section. In section 3, we discuss the thermal phase transition in detail. In section 4, we discuss how EWBG can be achieved in this model via the local baryogenesis mechanism. A quick review of local electroweak baryogenesis is presented. Section 5 provides UV completion. In section 6, we discuss how to probe this model in various experiments and astrophysical observations. Finally, we summarize this work in section 7.

2 The model

2.1 The tree-level potential

The Higgs doublet is decomposed as

$$H = \frac{1}{\sqrt{2}} \begin{pmatrix} \chi_1 + i\chi_2 \\ h + i\chi_3 \end{pmatrix}, \tag{2.1}$$

JHEP04(2024)108

where h is the physical Higgs field that obtains the vev $\langle h\rangle = \sqrt{2}v$ and $\chi_{1,2,3}$ are the would-be Nambu-Goldstone modes. The ALP-Higgs scalar potential in eq. (1.1) is written as

$$V = -\frac{1}{2}(\mu_H^2 - Af\cos\delta)h^2 + \frac{1}{4}\lambda h^4 + \mu_S^2 f^2\left(1-\cos\left(\frac{S}{f}\right)\right) - \frac{1}{2}Af\left(h^2-2v^2\right)\cos\left(\frac{S}{f}-\delta\right). \tag{2.2}$$

The periodicity in S of the third and fourth terms can be in general different from each other, but we consider the case with the same periodicity. The UV completion presented in section 5 indeed gives the same periodicity. We take $\delta \in [-\pi, \pi]$ without loss of generality. Noticing the spurious symmetry $S \to -S$ and $\delta \to -\delta$ in the potential, we may further take $\delta \in [0, \pi]$. For $\delta > \pi/2$, we find that the electroweak vacuum with $\langle h\rangle \simeq \sqrt{2}v$ is not the absolute minimum, and there exists a deeper minimum with larger $\langle h\rangle$. We may redefine the parameters so that at that minimum $\langle h\rangle = \sqrt{2}v$, and the corresponding δ after the shift of S to set $S = 0$ becomes smaller than $\pi/2$. In conclusion, we only concentrate on $0 \le \delta \le \pi/2$.

The would-be Nambu-Goldstone boson masses and the physical scalar mass matrix are

$$\begin{aligned} m_{\rm gs}^2 &= \lambda h^2 - \mu_H^2 - Af\cos\left(\frac{S}{f}-\delta\right) + Af\cos\delta, \\ m_{h,S}^2 &= \begin{pmatrix} m_{hh}^2 & m_{hS}^2 \\ m_{hS}^2 & m_{SS}^2 \end{pmatrix} \\ &\equiv \begin{pmatrix} 3\lambda h^2 - \mu_H^2 - Af\cos\left(\frac{S}{f}-\delta\right) + Af\cos\delta & Ah\sin\left(\frac{S}{f}-\delta\right) \\ Ah\sin\left(\frac{S}{f}-\delta\right) & \mu_S^2\cos\frac{S}{f} + \frac{A}{2f}(h^2-2v^2)\cos\left(\frac{S}{f}-\delta\right) \end{pmatrix}. \end{aligned} \tag{2.3}$$

The h and S boson mass squares are the eigenvalues of the mass matrix,

$$m_\pm^2 = \frac{1}{2}\left(m_{hh}^2 + m_{SS}^2 \pm \sqrt{(m_{hh}^2 - m_{SS}^2)^2 + 4m_{hS}^4}\right). \tag{2.4}$$

We consider the case where the heavier mass eigenstate with a mass square m_+^2 is the SM-like Higgs, and the lighter one is a new state.

The free parameters in this Lagrangian are $\{\lambda, \mu_H, \mu_S, A, f, \delta\}$. While keeping δ and f as free parameters, we express the remaining four by other quantities that are directly observable: the Higgs vev $v \simeq 174\,\text{GeV}$, the Higgs mass $m_h \simeq 125\,\text{GeV}$, the ALP mass m_S, and the mixing angle between the ALP and Higgs θ. At the tree level, the relation is given by

$$\begin{aligned} A &= \frac{1}{2\sqrt{2}v}(m_h^2 - m_S^2)\sin(2\theta)\csc(\delta), \\ \lambda &= \frac{1}{8v^2}\left(m_h^2 + m_S^2 + (m_h^2 - m_S^2)\cos(2\theta)\right), \\ \mu_H^2 &= \frac{1}{4}\left(m_h^2 + m_S^2 + (m_h^2 - m_S^2)\cos(2\theta)\right), \\ \mu_S^2 &= \frac{1}{2}\left(m_h^2 + m_S^2 - (m_h^2 - m_S^2)\cos(2\theta)\right). \end{aligned} \tag{2.5}$$

Matching $A\sin\delta$ in this model with A' in the simplified model, eq. (2.5) is exactly the same as the parametrization in the simplified model [34, 52]. For example, at a benchmark point

JHEP04(2024)108

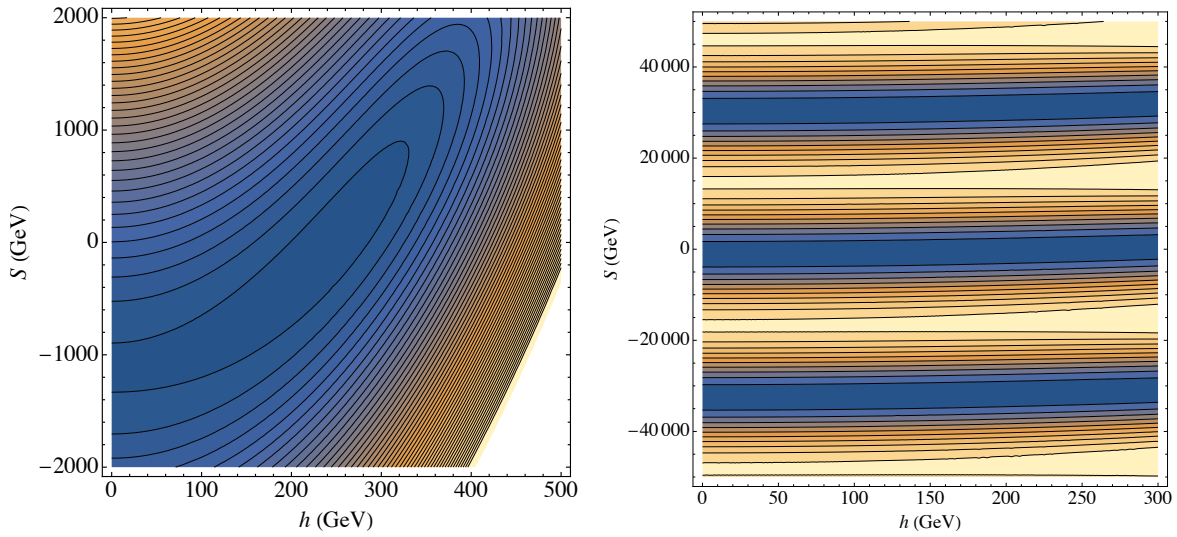

Figure 1. Tree-level potential for a benchmark point with $f = 5\,\text{TeV}$, $\delta = 2\pi/5$, $m_S = 5\,\text{GeV}$, and $\sin\theta = 0.1$. Left: potential in a small range of S. One can clearly see the "valley" that passes through the point $(\sqrt{2}v, 0)$. Right: potential in a wider range of S. One can see the periodicity of the potential along the S direction.

$f = 5\,\text{TeV}$, $\delta = 2\pi/5$, $m_S = 5\,\text{GeV}$, and $\sin\theta = 0.1$, eq. (2.5) gives

$$A = 6.65\,\text{GeV},\ \mu_S^2 = 181.325\,\text{GeV}^2,\ \mu_H^2 = 7750.6\,\text{GeV}^2,\ \lambda = 0.128. \tag{2.6}$$

The potential shape at this benchmark point is plotted in figure 1.

To get the path that minimizes the potential, i.e., the "valley" of the potential in the $h - S$ space, we take $\partial V/\partial S = 0$. The field value of S along this path can be written as

$$S(h) = f \arctan\left(\frac{A(h^2 - 2v^2)\sin(\delta)}{2f\mu_S^2 + A(h^2 - 2v^2)\cos(\delta)}\right). \tag{2.7}$$

The field value shift of S when h shift from 0 to $\sqrt{2}v$ is thus roughly

$$\Delta S \simeq \frac{A}{\mu_S^2} v^2 \sin\delta. \tag{2.8}$$

where the large f limit was taken.

When $\Delta S \ll f$, the dynamics of the model can be well-described by the simplified model, while as ΔS gets closer to f, the deviation from the simplified model becomes significant and the phase transition may be affected. We thus define the critical decay constant f_c via

$$f_c \equiv \frac{A}{\mu_S^2} v^2 \sin\delta, \tag{2.9}$$

and parameterize f as $f \equiv c f_c$. When scanning over the parameter space, we use c instead of f as a free parameter. f_c is defined by the tree-level parameters. The one-loop parameters are then solved from this f_c, following the framework discussed in the next subsection.

JHEP04(2024)108

We require $V(\sqrt{2}v, S(\sqrt{2}v)) < V(0, S(0))$ for the stability of the EW vacuum. The precise expression is complicated, but it roughly behaves as $\mu_S^2 f^2 > Av^2 f$ in large f limit. Expressing f by c, the bound is

$$c \sin\delta > 1. \tag{2.10}$$

This lower bound on c strongly constrains the model. Numerical computation indeed shows that c slightly below this value will lead to the violation of the stability requirement for almost all the parameter space. As will be discussed in section 3, c needs to be as small as possible to achieve a stronger phase transition. In the parameter space with small δ, increasing c is necessary. This will be discussed in detail in section 3. In addition, since the precise expression of the condition is not exactly eq. (2.10), especially when 1-loop quantum correction is taken into account, we numerically check the stability requirement during parameter scanning, and show the excluded parameter space in gray shaded region in figure 5 and 6.

For small c, the UV cutoff of the theory is strongly constrained by naturalness. The quantum correction to the potential of S by the Higgs loop is

$$\Delta\mu_S^2 \sim \frac{\Lambda_H^2}{16\pi^2}\frac{A}{f}, \tag{2.11}$$

where Λ_H is the cutoff of the loop integral. We require that $\Delta\mu_S^2 < \mu_S^2$. Using $f = cf_c$ and eq. (2.9), this condition becomes

$$\Lambda_H < 4\pi v\sqrt{c\sin\delta}. \tag{2.12}$$

For $c\sin\delta = O(1)$, the cutoff should be around the TeV scale. This does not necessarily require the significant modification of the Higgs itself around the TeV scale by such as supersymmetry or compositeness of the Higgs. In section 5, we present models where the cutoff is provided by the compositeness of S or new fermions and collective symmetry breaking.

2.2 One-loop corrections

The scalar potential receives quantum corrections. At the one-loop level, the Coleman-Weinberg (CW) potential [79] under the $\overline{\text{MS}}$ renormalization scheme is

$$V_{\text{CW}} = \frac{1}{64\pi^2}\left(\sum_B n_B\left(\log\left(\frac{m_B^2(h,S)}{Q^2}\right) - c_B\right) - \sum_F n_F\left(\log\left(\frac{m_F^2(h,S)}{Q^2}\right) - c_F\right)\right), \tag{2.13}$$

where B, F is for bosons and fermions, and $n_{B,F}$ is the degrees of freedom. The constant $c_B = 3/2$ for longitudinal gauge bosons and scalar bosons, and $c_B = 1/2$ for transverse gauge bosons. For fermions, $c_F = 3/2$. Q is the renormalization scale.

The gauge and top Yukawa couplings are renormalized under the $\overline{\text{MS}}$ renormalization scheme at $Q = m_Z = 91.1876\,\text{GeV}$. The input parameters to compute those parameters are $m_W = 80.379\,\text{GeV}$, $m_t = 172.69\,\text{GeV}$, $\alpha_3 = 0.1184$, $m_h = 125.13\,\text{GeV}$, and $G_F = 1.1663787 \times 10^{-5}\,\text{GeV}^{-1/2}$. The one-loop $\overline{\text{MS}}$ parameters are computed following the expressions in ref. [80]. The quantum corrections from the couplings involving S are negligible because of

JHEP04(2024)108

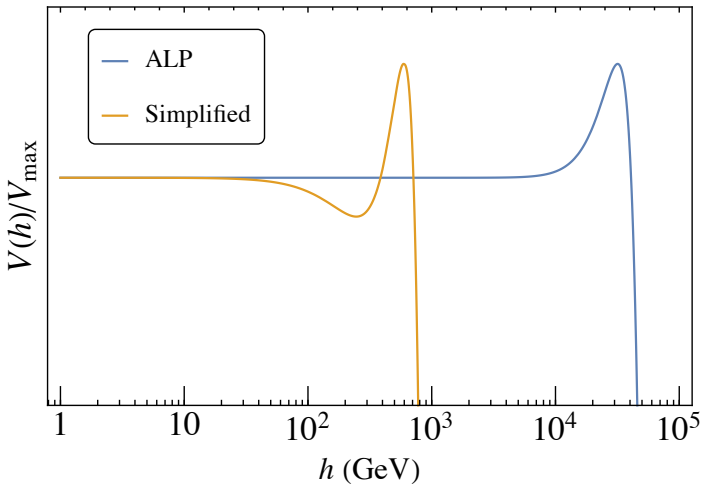

Figure 2. Comparison of the potential $V(h)$ along the path $\partial V/\partial S = 0$ between the full ALP model and the simplified model. The potential value is normalized by the value at the peak $V_{\max}$ of each one, about $10^{15}\,\mathrm{GeV}^4$ for the ALP model while $10^7\,\mathrm{GeV}^4$ for the simplified model.

the weak coupling. The parameters at a benchmark point $f = 5\,\mathrm{TeV}$, $\delta = 2\pi/5$, $m_S = 5\,\mathrm{GeV}$, and $\sin\theta = 0.1$ is

$$A = 6.69\,\mathrm{GeV}, \quad \mu_S^2 = 181.51\,\mathrm{GeV}^2, \quad \mu_H^2 = 8765.52\,\mathrm{GeV}^2, \quad \lambda = 0.1495. \tag{2.14}$$

The large negative contribution from the top quark in eq. (2.13) may destabilize the EW vacuum. The interaction between h and S makes the potential of h along the valley flatter than the SM. The quantum correction from the top then makes the potential energy turn down at a field value of h not much above the EW scale. We, however, found that the EW vacuum is stable enough. A comparison can be made with the simplified model, whose stability was confirmed in ref. [52]. A small effective quartic coupling along the "valley" appears in the simplified model so that the effective potential at $T = 0$ starts to turn down at around $h = 500\,\mathrm{GeV}$, potentially leading to the instability problem of the EW vacuum. However, the tunneling rate from the EW vacuum to large field values through the barrier is suppressed by the large tunneling action S_4 due to the scalar kinetic energy; from eq. (2.8), one can see that the field value shift of S is huge for light ALPs, which contributes extra large kinetic energy to the tunneling action. Such suppression also happens in thermal phase transition, as discussed in section 3.2. This large tunneling action protects the stability of the EW vacuum. In the full ALP model, the path $\partial V/\partial S = 0$ is less flat because of the cosine coupling between S and H rather than a linear one, pushing the turning point where the effective potential starts to drop to a much higher field value, roughly 2 order of magnitude higher than that in the simplified model. For example, in figure 2, we show the comparison of the potential as a function of h along $\partial V/\partial S = 0$ path between the ALP model and the simplified model at the benchmark point in eq. (2.14). The barrier between the metastable EW vacuum and the infinity appears around $h \simeq 600\,\mathrm{GeV}$ in the simplified model, while $h \simeq 30\,\mathrm{TeV}$ in the full model. The peak height is about $10^{15}\,\mathrm{GeV}^4$, compared to $10^7\,\mathrm{GeV}^4$ of the simplified model. The S field value in the ALP model is similar to the simplified model at

JHEP04(2024)108

least until the escape point of the simplified model. In conclusion, like the simplified model, the tunneling action of the ALP model is large because of the large change of the S field value, and the high potential barrier and large change of the Higgs field value will further increases the tunneling action, resulting in an EW vacuum even more stable than the simplified model.

3 The electroweak phase transition

3.1 Finite temperature corrections

In addition to eq. (2.13), the scalar potential receive finite-temperature correction term when $T > 0$ (see [53] for a review)[2]

$$V_{\rm FT} = \frac{T^4}{2\pi^2}\left(\sum_B n_B J_B\left(\frac{m_B^2(h,S)}{T^2}\right) + \sum_F n_F J_F\left(\frac{m_F^2(h,S)}{T^2}\right)\right),$$
$$J_{B,F}(x^2) = \pm\int_0^\infty dy\; y^2 \log\left(1 \mp \exp\left(-\sqrt{y^2+x^2}\right)\right). \tag{3.1}$$

When the mass is not large compared with the temperature, we can use the high-temperature expansion of the integral function $J_{B,F}$. This approximation is not well-justified for a strong first-order phase transition, but it provides qualitative information. Here we apply the high-temperature expansion as a quick, qualitative look for the finite temperature effective potential, while for the numerical computations we always use the full expressions. Under the high-temperature expansion, the total effective potential becomes

$$\begin{aligned} V_{\rm highT} = &-\frac{1}{2}(\mu_H^2 - Af\cos\delta)h^2 + D_{\rm SM}T^2h^2 - E_{\rm SM}Th^3 - E(h,S)T + \frac{1}{4}\lambda h^4 \\ &- \frac{1}{2}Af\cos\left(\frac{S}{f}-\delta\right)\left(\left(h^2 - 2v^2 + \frac{1}{3}T^2\right) - \frac{T^2}{24f^2}\left(h^2-2v^2\right)\right) \\ &- \left(1 - \frac{T^2}{24f^2}\right)\mu_S^2 f^2\cos\left(\frac{S}{f}\right), \end{aligned} \tag{3.2}$$

where the Standard Model coefficients are

$$D_{\rm SM} = \frac{1}{32}\left(3g^2 + g_1^2 + 4y_t^2 + 8\lambda\right),$$
$$E_{\rm SM} = \frac{1}{32\pi}\left(2g^3 + (g^2+g_1^2)^{3/2}\right). \tag{3.3}$$

Among the corrections from the couplings involving S, the term proportional to $T^2/3$ in the second line of eq. (3.2) is the dominant effect. The term $E(h,S)$ comes from the IR singularity of the scalar boson contribution, as $E_{\rm SM}$. The exact form is complicated but roughly behaves as $(Af\cos(S/f-\delta))^{3/2}$. This term contributes positively to the phase transition strength, but is smaller than or at most comparable with other terms and does not have a qualitative impact on the potential shape. We thus neglect this term in our high-temperature, analytical discussion. (Full scalar contributions are included in the numerical computations). The term

[2]Notice that the sign convention in J_F and n_F is different from [53].

JHEP04(2024)108

proportional to T^2/f^2 in the second and third lines is also small due to the large f and thus can be neglected. Under these approximations, the high-temperature expanded potential becomes

$$\begin{aligned} V_{\text{highT}} = &-\frac{1}{2}(\mu_H^2 - Af\cos\delta)h^2 + D_{\text{SM}}T^2h^2 - E_{\text{SM}}Th^3 + \frac{1}{4}\lambda h^4 \\ &- \frac{1}{2}Af\cos\left(\frac{S}{f} - \delta\right)\left(h^2 - 2v^2 + \frac{1}{3}T^2\right) \\ &- f^2\mu_S^2\cos\left(\frac{S}{f}\right). \end{aligned} \tag{3.4}$$

Even for the case where the gauge bosons and fermions are not light compared with the temperature, eq. (3.4) can provide a qualitative intuition. The thermally generated h^3 barrier is the same as the SM (up to the additional subdominant $E(h,S)$ term), but the enhancement of the EWPT strength can come the zero-temperature potential, as discussed in the next subsection.

The "valley" now becomes

$$S(h,T) = f\arctan\left(\frac{A(3(h^2-2v^2)+T^2)\sin(\delta)}{6f\mu_S^2 + A(3(h^2-2v^2)+T^2)\cos(\delta)}\right). \tag{3.5}$$

Again, one can retrieve the path in the simplified model by taking $f \to \infty$,

$$S(h,T) = \frac{1}{2}\frac{A}{\mu_S^2}\left(h^2 - 2v^2 + \frac{1}{3}T^2\right)\sin\delta. \tag{3.6}$$

This shows that for any high temperature T and Higgs field h, S always has a single minimum. When the Higgs field vev is fixed at $\langle h\rangle = 0$ at high temperature, the global vev goes to $(0, S(0,T))$. Thus the phase transition is a simple one-step one with $(0,S(0,T)) \to (v(T), S(v(T),T))$.

In addition to eqs. (2.2), (2.13) and (3.1), we need to include the ring diagram contribution to resum the effective potential in order to keep the validity of the perturbative computation. This requires adding the thermal corrections to the boson masses in eqs. (2.13) and (3.1). The one coming from the gauge bosons is the same as the SM result, i.e.,

$$\begin{aligned} m^2_{A_L,Z_L} =& \begin{pmatrix} \frac{1}{4}g^2h^2 + \frac{11}{6}g^2T^2 & -\frac{1}{4}gg_1h^2 \\ -\frac{1}{4}gg_1h^2 & \frac{1}{4}g_1^2h^2 + \frac{11}{6}g_1^2T^2 \end{pmatrix}, \\ m^2_{Z_T} =& \frac{1}{4}(g^2+g_1^2)h^2, \\ m^2_{A_T} =& 0, \\ m_{W_L^\pm} =& \frac{1}{4}g^2h^2 + \frac{11}{6}g^2T^2, \\ m^2_{W_T} =& \frac{1}{4}g^2h^2, \end{aligned} \tag{3.7}$$

where the subscript L, T are for longitudinal and transverse modes, respectively. The A_L and Z_L boson masses are the eigenvalues of the mass matrix $m_{A,Z}$. Note that only the longitudinal mode of the gauge bosons receives the thermal mass corrections $\Pi \sim g^2T^2$. The

JHEP04(2024)108

thermal mass matrix for the scalar bosons can be derived from eq. (3.4). The $(1,1)$ and $(2,2)$ component of the mass matrix in eq. (2.3) receives thermal mass corrections,

$$\Pi_{hh} = 2D_{\rm SM}T^2, \Pi_{SS} = \frac{A}{2f}\cos(S/f-\delta)\times\frac{1}{3}T^2. \tag{3.8}$$

The thermal correction Π_{hh} also applies to the would-be Nambu-Goldstone bosons.

Throughout this paper, all numerical computations for the thermal phase transition are performed following the above computed one-loop thermal effective potential with resummation, i.e., eqs. (2.2), (2.13) and (3.1) with eqs. (3.7) and (3.8) included. Again, high-temperature expansion is never employed in the numerical computations.

3.2 Phase transition and bubble nucleation

At the critical temperature T_c, the thermal potential is degenerate for the false vacuum $(0, S(0,T_c))$ and the true vacuum $(v(T_c), S(v(T_c),T_c))$. As the universe continues cooling down, a thermal phase transition from the false vacuum to the true vacuum is kinetically allowed. Once the transition rate is larger than the Hubble rate, first-order phase transition proceeds via bubble nucleation. The criteria for such a condition is [53, 81]

$$\left.\frac{S_3}{T}\right|_{T_n} \simeq 140. \tag{3.9}$$

The temperature T_n when such a condition is satisfied is referred to as the nucleation temperature. The 3-dim Euclidean action, S_3, is the sum of the potential energy and the kinetic energy of both scalar fields,

$$S_3 = 4\pi\int r^2\left(\frac{1}{2}\left(\frac{dh(r)}{dr}\right)^2+\frac{1}{2}\left(\frac{dS(r)}{dr}\right)^2+V(h(r),S(r))\right). \tag{3.10}$$

Here r is the space coordinate and the integral is performed along the bubble profile whose $h(r)$ and $S(r)$ minimize such an action. Numerical computation shows that the path (i.e., the profile) of the thermal phase transition is always almost along the "valley" where $\partial V/\partial S = 0$. In figure 3, we show the field value shift of h and S for a benchmark point $m_S = 5\,\text{GeV}$, $\sin\theta = 0.07$, $c = 3$, and $\delta = 2\pi/5$.

From eq. (3.6), one can see that the field value shift of S is larger for a smaller scalar mass. Such a large field value shift will contribute huge kinetic energy to eq. (3.10), as discussed in the previous paper [52]. Another important quantity is the inverse time duration, defined as

$$\frac{\beta}{H} \equiv T_n\left.\frac{d}{dT}\left(\frac{S_3}{T}\right)\right|_{T_n}. \tag{3.11}$$

In the left panel of figure 4, we show β/H as a function of m_S. The mixing angle is derived by fixing the tuning parameter $m_S^2/\mu_S^2 = 13\%$. Numerical computations of the effective potential and thermal phase transition action are performed with the help of `cosmoTransitions` [82]. Here "2d" is the result of the full two-field dynamics, while "1d" is the result of a truncated computation where the path is confined to the 1-dimensional valley and the kinetic term of S is neglected. One can see that the β/H parameter increases quickly as m_S decreases for

JHEP04(2024)108

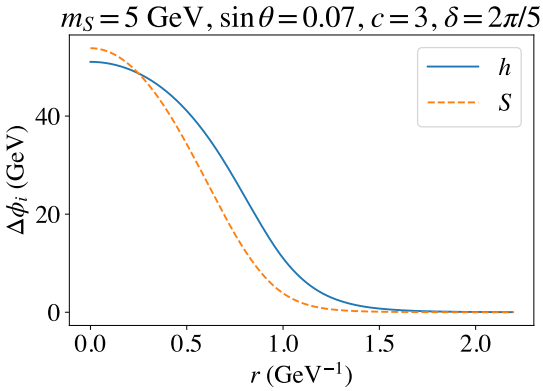

Figure 3. Wall profile during phase transition for a benchmark point $m_S = 5\,\text{GeV}$, $\sin\theta = 0.07$, $c = 3$ and $\delta = 2\pi/5$. The change of the field value $\Delta\phi_i = \Delta h, \Delta S$, is defined so that they are 0 for $r \to \infty$.

the full 2-dim computation. The truncated 1-dim computation significantly underestimates β/H if $m_S < 10\,\text{GeV}$.

β/H is large for the following reason. Because of the weak coupling of S, each term in S_3 is large. Around the nucleation temperature, the large positive contribution from the kinetic energy of S and h cancels with the large negative contribution from the potential, and thus $S_3/T \simeq 140$ is achieved. However, this cancellation does not occur for their derivatives, causing huge β/H. The large β/H parameter has significant impacts. A large β/H corresponds to a short time duration of the phase transition, which suppresses the gravitational-wave signals.

A large β/H also implies a rapid decrease of the tunneling action S_3 as the temperature drops. Such a rapid change compensates for the large S_3 coming from the huge field value shift of S, preventing the nucleation temperature from being much below the critical temperature. In the right panel of figure 4, we show the comparison between T_n and T_c as a function of m_S. T_n deviates more from T_c for the 2-dim computation, but the difference is still below one percent.

A SFOPT is defined as a FOPT such that the sphaleron processes decouple in the broken phase, i.e., the sphaleron rate at the T_n in the broken phase is smaller than the Hubble rate. For the computation of the sphaleron rate, see [83, 84]. Rather than the commonly used SFOPT criteria $v_c/T_c \geq 1$, the physical criteria for SFOPT should be $v_n/T_n \geq 1$, and sometimes they can favor very different parameter spaces [85]. In this model, however, we numerically found that

$$\frac{v_n}{T_n} \simeq 1.2\frac{v_c}{T_c}. \tag{3.12}$$

To speed up the computation and avoid numerical fluctuations, we numerically compute v_c/T_c, use eq. (3.12) to estimate v_n/T_n, and then require $v_n/T_n \geq 1$ for the SFOPT. Prediction on the minimal $\sin\theta$ for a certain m_S for SFOPT under $v_c/T_c \geq 1$ and $v_n/T_n \geq 1$ differ from each other by less than 10%.

In figure 5, we showed the bound on the model for several choices of (c, δ). In the blue-shaded regions, the SFOPT is not achieved. Computation and numerical scanning for the

JHEP04(2024)108

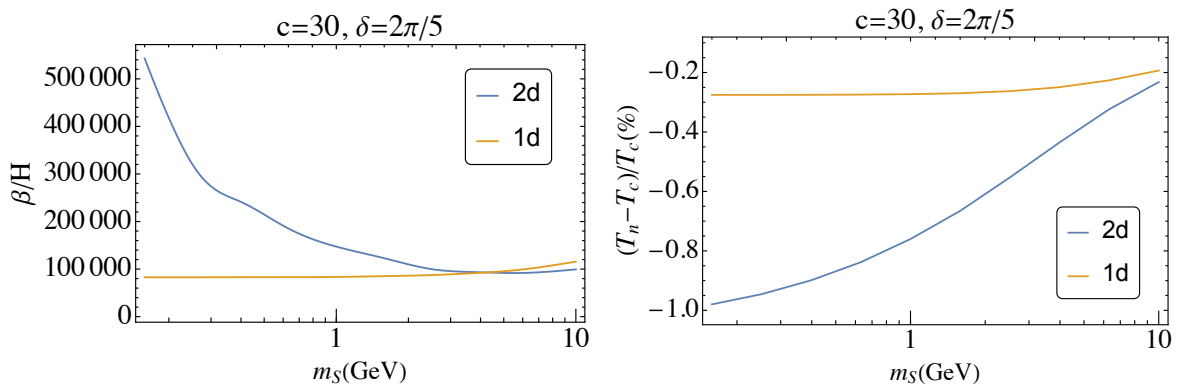

Figure 4. Properties of the phase transition. The mixing angle θ is fixed so that $m_S^2/\mu_S^2 = 0.13$. "2d" is the result of the full two-field dynamics. "1d" is the result of the approximation where the path is fixed on the valley of potential and the kinetic term of S is neglected. Left: the inverse duration of the phase transition, β/H. One can see that it blows up for small m_S. Right: the difference between nucleation temperature T_n and the critical temperature T_c normalized by T_c. One can see that the nucleation temperature is more delayed for smaller m_S, but the delay is less than 1% and the increase of the delay gradually slows down for the MeV scale m_S.

critical temperature are performed with a Python code, and cross-checked with a `Mathematica` code for a few parameter points. Among them, $c = 3, \delta = \pi/5$ and $c = 3, \delta = 2\pi/5$ requires $\Lambda_H \lesssim$ few TeV. Increasing c by 10 times for fixed δ relaxes this upper bound for Λ_H by a factor of $\sqrt{10}$. Via numerical computation, we find that the ratio $\Delta S/f$ during phase transition becomes smaller for $c < 3$, which in turn leads to a weaker PT strength, thus we do not explore smaller c for $\delta = 2\pi/5, \pi/5$. For smaller δ, $c = 3$ violates the EW stability requirement in eq. (2.10). For this reason, for $\delta = \pi/20$ we take $c = 1.2/\sin\delta$ and $c = 1.5/\sin\delta$ in figure 5. These values of c require $\Lambda_H \lesssim$ few TeV. As δ becomes smaller with $(m_S, \sin\theta, c\sin\delta)$ fixed, v_c/T_c slowly increases up to by 10%, but this does not change the lower bound on the mixing angle beyond the uncertainty of our computation discussed below.

Our computation includes the one-loop zero-temperature CW potential and the one-loop finite temperature corrections with resummation. Including the CW correction is important. Indeed, if we remove the CW potential and use the tree-level zero-temperature potential, v_c/T_c increases by an $O(1)$ factor and reach even ~ 3. The prediction on the mixing angle changes correspondingly.

However, this computation method, though commonly used in this community, still suffers from large computational uncertainties. As discussed in the appendix, higher-loop thermal corrections increase the prediction on v_c/T_c in the SM with a lighter Higgs by as much as 50% in comparison with the one-loop computation. A similar enhancement of the PT strength may happen in the ALP model. A careful two-loop computation is required in the future to make a more convincing prediction but is beyond the scope of the current paper. (The publicly available code `DRalgo` package [56] cannot treat cosine potentials.) If v_c/T_c is actually larger than the prediction of the one-loop computation by 50%, the predicted SFOPT lower bound on $\sin\theta$ for each ALP mass may be relaxed by about 20% for $c\sin\delta = O(1)$.

JHEP04(2024)108

3.3 Enhancement of the phase transition

To see how EWPT strength is enhanced in comparison with the SM and the simplified model, we work up to order $Af^{-1}S^2h^2\cos\delta$. We see that the "valley" at $T=0$ is now expressed as

$$\begin{aligned} S &= \frac{Af(h^2-2v^2)\sin\delta}{2f\mu_S^2+A(h^2-2v^2)\cos\delta} \\ &\simeq \frac{Afv^2\sin\delta}{Av^2\cos\delta-f\mu_S^2}+\frac{Af^2\mu_S^2\sin\delta}{2(Av^2\cos\delta-f\mu_S^2)^2}h^2+\frac{A^2f^2\mu_S^2\sin\delta\cos\delta}{4(Av^2\cos\delta-f\mu_S^2)^3}h^4+O(h^6). \end{aligned} \tag{3.13}$$

Along this path, the 1-dim tree-level potential has a positive h^6 term, while the quartic term is

$$\frac{1}{4}\left(\lambda-\frac{A^2f^3\mu_S^4\sin^2\delta}{2(\mu_S^2f-Av^2\cos\delta)^3}\right)h^4. \tag{3.14}$$

Since we assume $\mu_S^2 f > Av^2$, the correction always makes this effective quartic coupling smaller than λ. However, when large A or small f is taken so that $\mu_S^2 f$ is not much above Av^2, the denominator of the correction term can be small so that the large correction may even make the effective quartic coupling negative. This negative h^4 term contributes an extra barrier in addition to the traditional thermal h^3 barrier, while the local minimum comes from the competition between the negative h^4 and positive h^6. This significantly enlarges the barrier and thus enhances the strength of EWPT. With numerical computations, we found that this is indeed the case in the parameter region where SFOPT is achieved.

The model requires mild tuning. After we express f in terms of cf_c following eq. (2.9), the correction in eq. (3.14) still behaves as $A^2/\mu_S^2 \propto (m_h^2-\mu_S^2)(1-m_S^2/\mu_S^2)$. A smaller m_S^2/μ_S^2 helps make the effective quartic coupling negatively large and achieve SFOPT. Small m_S^2/μ_S^2 requires mild tuning of parameters. For example, the benchmark point in eq. (2.6) has $m_S^2/\mu_S^2 = 0.14$. The SFOPT boundary in the parameter space is almost parallel with a contour for a fixed m_S^2/μ_S^2, depending on the c and δ. For example, the SFOPT boundary for $c=3$ and $\delta = 2\pi/5$ has roughly 25% tuning.

4 Local electroweak baryogenesis

In local electroweak baryogenesis, the CP violation and B violation occur at the same local spacetime during the electroweak phase transition as the wall passes through. We first briefly review the mechanism in a general way, following ref. [65, 66]. Consider an operator $\hat{\mathcal{O}} = \alpha_2\theta W\tilde{W}/(8\pi)$ or $\hat{\mathcal{O}} = \partial_\mu\theta\psi^\dagger\bar{\sigma}^\mu\psi$, where W is the field strength of the SU(2) gauge field, ψ is an SU(2) doublet fermion, and θ depends on some fields whose field values shift during the phase transition. In the thick-wall regime where the wall thickness is much larger than the mean free path of the particles, θ changes slowly and we may assume a small departure from local thermal equilibrium. The time-dependence of θ gives the imbalance between the sphaleron and anti-sphaleron rates via this operator, and the net baryon number is produced. This can be understood by the effective chemical potential of the Chern-Simons number of W or the fermion number of ψ, with an equilibrium value of the baryon number $n_B^0 \sim \dot{\theta}T^2$. See [86, 87] for the Boltzmann equation of the SM particles under $\dot{\theta} \neq 0$. We may then

JHEP04(2024)108

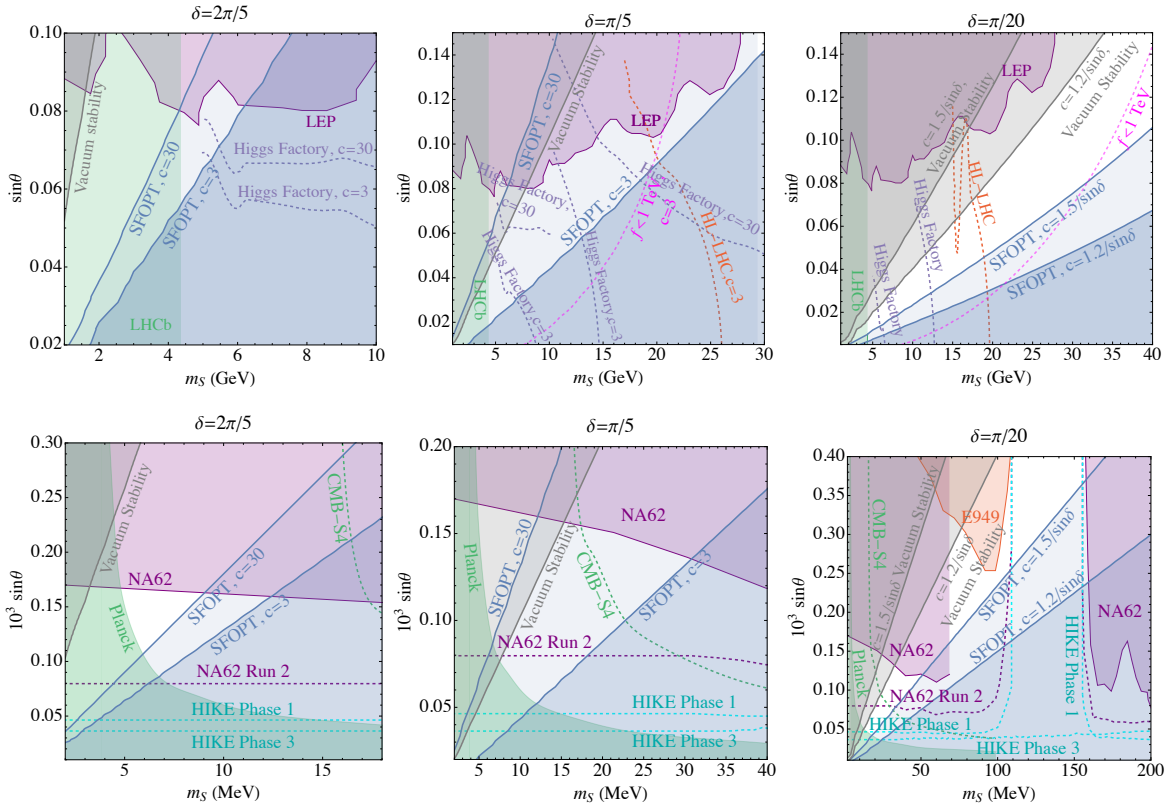

Figure 5. Parameter space in $m_S - \sin\theta$ plane for different c and δ. Upper panels: m_S in the GeV scale. For $\delta = \pi/20$, the Higgs exotic search projection curve and $f = 1$ TeV curve for $c = 1.2/\sin\delta$ and $c = 1.5/\sin\delta$ are very close to each other and we only show the curves for $c = 1.2/\sin\delta$. Lower panels: m_S in the MeV scale. Gray shaded region: excluded by vacuum stability requirement $V(0) > V(\sqrt{2}v)$. For $\delta = \pi/5$ or $2\pi/5$, this requirement is only plotted for $c = 3$. The curve for $c = 30$ is outside the plot range.

determine the evolution of the baryon asymmetry from the detailed balance principle,

$$\dot{n}_B \propto -\Gamma_{\rm sph}(n_B - n_B^0). \tag{4.1}$$

where $\Gamma_{\rm sph} \simeq 20\alpha_W^5 T$ is the sphaleron rate per volume. Since the sphaleron rate is highly suppressed by α_W^5, the produced baryon number n_B is always much smaller than the $\dot{\theta}T^2$ and thus we can ignore n_B on the right-hand side of this equation. Integrating over time, we obtain

$$n_B \propto \Gamma_{\rm sph} T^2 \Delta\theta, \tag{4.2}$$

where $\Delta\theta$ is the shift of θ from outside the bubble wall to inside until the sphaleron rate is suppressed.

Local electroweak baryogenesis was considered for dim-6 operator $|H|^2 W\tilde{W}/M^2$ in ref. [65, 66], where M is a dimensionful parameter. Here, θ is identified with $|H|^2/M^2$. However, as stated in the introduction, M must be right above the weak scale because of the small field value shift of h. On the other hand, in our model, we may instead consider

JHEP04(2024)108

the following dim-5 operators,

$$\mathcal{L} = \frac{\alpha_2}{8\pi} c_W \frac{S}{f} W\tilde{W}, \quad \frac{\partial_\mu S}{f} c_{q_{ij}} q_i^\dagger \bar{\sigma}^\mu q_j, \quad \text{or} \quad \frac{\partial_\mu S}{f} c_{\ell_{ij}} \ell_i^\dagger \bar{\sigma}^\mu \ell_j, \tag{4.3}$$

where q and ℓ are quark and lepton doublets, respectively. c_W, $c_{q_{ij}}$ and $c_{\ell_{ij}}$ are coupling constants. We can take $c_{\psi_{ij}} = \delta_{ij} c_{\psi_i}$ by unitary rotations of fermion fields, where $\psi = q$ or ℓ. The coupling with W is also discussed in ref. [51]. These effective operators can be generated by UV physics as will be discussed in section 5. The $SW\tilde{W}$ coupling is generated through the weak anomaly of the shift symmetry of S, while the $(\partial S)\psi^\dagger\bar{\sigma}\psi$ coupling is generated through a non-zero U(1) charge of SM fermions or the mixing of SM fermions with U(1)-charged heavy fermions. The large field value shift of S during the phase transition means that the required value of f for a successful baryogenesis is large, so that the electron EDM constraint is avoided.

Here, we follow the computation in ref. [86, 87] to derive the Boltzmann equation for n_q. Defining n_{q_i} to contain all the colors of quark doublets for each generation, the part of the Boltzmann equation relevant for baryogenesis can be written as

$$\dot{n}_{q_i} = 9\Gamma_{\rm sph} \sum_j \left(-n_{q_j} - n_{\ell_j} + \frac{3c_{q_j} + c_{\ell_j} - c_W/3}{3} \dot{\theta} T^2 \right), \tag{4.4}$$

where the overall coefficient 9 is derived from the result in ref. [88]. The baryon number is thus

$$n_B = \Gamma_{\rm sph} T^2 \frac{\Delta S}{f} \sum_i (9c_{q_i} + 3c_{\ell_i} - c_W). \tag{4.5}$$

If $c_W = 1$ and $c_{q_i} = c_{\ell_i} = 0$, we find that the BAU produced in the viable parameter space is larger than the observed one by an $O(1-10)$ factor for $c = 1.5/\sin\delta$ with small δ and $c = 3$ for $\delta = \pi/5$, and by an $O(20-50)$ factor for $c = 1.2/\sin\delta$ with $\delta = \pi/20$. For larger c and δ, the produced BAU can be smaller and reach the observed amount. For example, the produced BAU is around the observed value for $c = 3, \delta = 2\pi/5$. For a model with $c_{q_i} = 1$ or $c_{\ell_i} = 1$ while $c_W = 0$, the produced baryon number is 9 or 3 times larger that the model with $c_W = 1$ and $c_{q,\ell} = 0$, respectively. Explaining the observed BAU for those overproduced cases requires suppression of the operators in eq. (4.3). The realization of the suppression in UV theories is discussed in the next section.

5 UV completion

In this section, we discuss the UV completion of the ALP-assisted model. In section 5.1, we present models where the ALP S arises by a spontaneous breaking in a QCD-like theory. The smallness of f in comparison with other fundamental scales is explained by the dimensional transmutation. As we will see, the model can be UV-completion for $m_S = O(10)\,\text{GeV}$. In section 5.2, we discuss a model where S is a phase direction of a fundamental complex scalar field. The model can be a UV completion for both $m_S = O(10)\,\text{MeV}$ and GeV, but does not explain the smallness of f in comparison with other fundamental scales. To explain it, the model should be further extended, e.g., with supersymmetry with a supersymmetry breaking scale at or below f. For $m_S = O(10)\,\text{MeV}$, where $f = O(10^{6-7})\,\text{GeV}$, this does not require low-scale supersymmetry. See ref. [51] for another UV-complete model.

JHEP04(2024)108

5.1 Composite UV completion

We first discuss a model where $SW\tilde{W}$ coupling is $\alpha_2/(8\pi f)$-suppressed without further suppression. The model is consistent with the parameter region where the observed BAU can be explained if $c_W \simeq 1$. We introduce an SU(N) gauge interaction ($N \geq 3$) with fermions shown in table 1. The SU(N) theory has 3 flavors, and the $\mathrm{SU}(3)_L \times \mathrm{SU}(3)_R$ global symmetry is broken down into $\mathrm{SU}(3)_V$, yielding the following 8 NGBs:

$$T(3,0),\ D(2,1/2),\ S(1,0), \tag{5.1}$$

where the numbers in the parenthesis denote the $\mathrm{SU}(2)_L \times \mathrm{U}(1)_Y$ charges. There is one neutral NGB S, and the corresponding spontaneously broken global U(1) charges of the fermions are also shown in table 1. U(1) has $\mathrm{SU}(2)_L \times \mathrm{U}(1)_Y$ anomaly, so S has anomalous couplings to the electroweak gauge bosons suppressed by $\alpha_2/(8\pi f)$. Non-zero masses of $L\bar{L}$ and $E\bar{E}$ give a non-zero mass to S.

We introduce the following couplings with the Higgs;

$$\mathcal{L} = yHL\bar{E} + \bar{y}H^\dagger \bar{L}E + \mathrm{h.c.} \tag{5.2}$$

These couplings violate U(1) and generate $H - D$ mass mixing whose phase depends on S. The exchange of D generates the couplings of S with the Higgs,

$$\frac{\Lambda_N^4}{16\pi^2}\frac{y\bar{y}}{m_D^2}e^{iS/f}|H|^2 + \mathrm{h.c.}, \tag{5.3}$$

where $\Lambda_N \sim 4\pi f$ is the dynamical scale of SU(N) and we determined the factor of 4πs by the naive dimensional analysis [89–91]. These terms are the origin of the $S - H$ coupling in eq. (1.1). The relative phase between $y\bar{y}$ and the masses of L and E gives non-zero δ. Closing the Higgs loop, a potential of S is generated,

$$\frac{\Lambda_N^4}{(16\pi^2)^2}y\bar{y}e^{iS/f}\ln\frac{\Lambda_N}{m_D}. \tag{5.4}$$

In terms of the effective theory in eq. (5.3), the Higgs loop has a cut-off at $\Lambda_H \sim m_D \sim gf$. For the parameter region with $m_S = O(10)\,\mathrm{GeV}$ where $f = O(1)\,\mathrm{TeV}$, the naturalness condition in eq. (2.12) is satisfied.

We next discuss a model where $SW\tilde{W}$ coupling is suppressed beyond $\alpha_2/(8\pi f)$, so that the observed BAU can be explained if overproduced for $c_W = 1$. We introduce an SU(N) gauge interaction ($N \geq 3$) with fermions shown in table 2. SU(N) has 4 flavors, and the $\mathrm{SU}(4)_L \times \mathrm{SU}(4)_R$ global symmetry is broken down into $\mathrm{SU}(4)_V$, yielding the following 15 NGBs:

$$T(3,0),\ D_1(2,1/2),\ D_2(2,1/2),\ S_c(0,1),\ S'(1,0), S(1,0) \tag{5.5}$$

There are two neutral NGBs S' and S, and the corresponding spontaneously broken global $\mathrm{U}(1)' \times \mathrm{U}(1)$ charges of the fermions are also shown in table 2. $\mathrm{U}(1)'$ has $\mathrm{SU}(2)_L \times \mathrm{U}(1)_Y$ anomaly, while U(1) does not, so S does not have anomalous couplings to the electroweak gauge bosons.

JHEP04(2024)108

	L	E	$\bar{L}$	$\bar{E}$
SU(N)	N	N	$\bar{N}$	$\bar{N}$
SU(2)$_L$	**2**	**1**	**2**	**1**
U(1)$_Y$	$-1/4$	$1/4$	$1/4$	$-1/4$
U(1)	1	-2	1	-2

Table 1. Fermion contents for a composite UV completion with unsuppressed $SW\tilde{W}$ coupling.

	L	E_+	E_-	$\bar{L}$	$\bar{E}_+$	$\bar{E}_-$
SU(N)	N	N	N	$\bar{N}$	$\bar{N}$	$\bar{N}$
SU(2)$_L$	**2**	**1**	**1**	**2**	**1**	**1**
U(1)$_Y$	0	$1/2$	$-1/2$	0	$-1/2$	$1/2$
U(1)	0	1	-1	0	1	-1
U(1)$'$	1	-1	-1	1	-1	-1

Table 2. Fermion contents for a composite UV completion with suppressed $SW\tilde{W}$ coupling.

Non-zero masses of S' and S are given by explicit U(1)$' \times$ U(1) breaking. A mass of $L\bar{L}$ only breaks U(1)$'$, and gives a mass only to S'. Nonzero masses of $E_+\bar{E}_+$ and $E_-\bar{E}_-$ break both U(1)$'$ and U(1), so give a mass to S as well as $S - S'$ mixing. Assuming $m_L \gg m_{E_\pm}$, we may achieve a hierarchy $m_{S'}^2 \gg m_S^2$ as well as a small $S - S'$ mixing. The small mixing introduces a small $SW\tilde{W}$ coupling required for the successful electroweak baryogenesis.

We introduce the following couplings with the Higgs;

$$\mathcal{L} = y_1 H L \bar{E}_+ + \bar{y}_1 H^\dagger \bar{L} E_+ + y_2 H^\dagger L \bar{E}_- + \bar{y}_2 H \bar{L} E_-. \tag{5.6}$$

These couplings preserve U(1)$'$ and S' does not couple to the Higgs. On the other hand, these couplings violate U(1) and generate $H - D_{1,2}$ mass mixing whose phase depends on S. The exchange of $D_{1,2}$ generates the couplings of S with the Higgs,

$$\frac{\Lambda_N^4}{16\pi^2} e^{iS/f} |H|^2 \left(\frac{y_1 \bar{y}_1}{m_{D_1}^2} + \frac{y_2 \bar{y}_2}{m_{D_2}^2} \right) + \text{h.c.}, \tag{5.7}$$

The relative phase between $y\bar{y}$ and the masses of E gives non-zero δ. Closing the Higgs loop, a potential of S is generated,

$$\frac{\Lambda_N^4}{(16\pi^2)^2} e^{iS/f} \left(y_1 \bar{y}_1 \ln \frac{\Lambda_N}{m_{D_1}} + y_2 \bar{y}_2 \ln \frac{\Lambda_N}{m_{D_2}} \right). \tag{5.8}$$

Again, the effective cutoff of the Higgs loop is $\Lambda_H \sim m_{D_{1,2}} \sim gf$.

Let us comment on the stability of composite particles in the two models described above. All of the mesons are unstable. The lightest SU(N) baryon is stable. If N is even, the lightest one is electroweak neutral and is a good dark matter candidate. With $f =$ few TeV, the mass of the baryon is expected by around several 10 TeV. The freeze-out of the annihilation of the baryon may explain the observed dark matter density.

In the two models described above, the SU(N) gauge theories have three and four light flavors respectively. It is considered that the phase transition of such SU(N) is of first order

JHEP04(2024)108

if $N \geq 3$ [92]. With the dynamical scale around 10 TeV, the phase transition temperature is also around 10 TeV. The resultant gravitational-wave signal may be observable.

5.2 Perturbative UV completion

We consider the following interactions and masses,

$$yP\bar{L}_1 L_2 + \lambda_1 H\bar{N}L_1 + \lambda_2 H^\dagger N\bar{L}_2 + m_1\bar{L}_1 L_1 + m_2\bar{L}_2 L_2 + m_N\bar{N}N, \tag{5.9}$$

where P is a complex scalar, $L_{1,2}$ and $\bar{L}_{1,2}$ are $\mathrm{SU}(2)_L$ doublet fermions, and N and $\bar{N}$ are singlet fermions. We assume a wine bottle potential of P. The angular direction of P is identified with S. This model is characterized by the collective symmetry breaking [93, 94], where the shift symmetry of S is violated only if all of y, λ_1, λ_2, m_1 m_2, and m_N are non-zero. For example, when $\lambda_1 = 0$, there is a U(1) symmetry under which $P(1)$, $L_1(-1)$, $\bar{L}_1(1)$, with other field having vanishing U(1) charges.

Because of the collective symmetry breaking, a one-loop correction to the $S - H$ coupling is finite:

$$\frac{y\lambda_1\lambda_2}{16\pi^2}\frac{m_1 m_2 m_N f}{\Lambda^2}e^{iS/f}|H|^2 + \text{h.c.}, \quad \Lambda = \max(y\langle P\rangle, m_1, m_2, m_N). \tag{5.10}$$

A two-loop correction to the potential of S, which arises as a tadpole term of P, is logarithmically divergent,

$$\frac{y\lambda_1\lambda_2}{(16\pi^2)^2}m_1 m_2 m_N f \ln\frac{\Lambda_c}{\Lambda}e^{iS/f} + \text{h.c.}, \tag{5.11}$$

where Λ_c is the cutoff of the model in eq. (5.9). One can see that $\Lambda_H \sim \Lambda$, which is given by the largest fermion mass scale. Even if $m_S = O(10)\,\mathrm{MeV}$, where $f = O(10^{6-7})\,\mathrm{GeV}$ is much above the upper bound on $\Lambda_H \sim$ few TeV, the Higgs loop may be cut off at the scale much below f, and the naturalness bound can be satisfied.

For $\lambda_{1,2} = 0$, the shift symmetry of S is exact as mentioned above, and the shift symmetry does not have an electroweak anomaly. This means that $SW\tilde{W}$ coupling vanishes when $H = 0$. Indeed, the determinant of the mass matrix of the electromagnetically charged fermions is independent of P, and that of the neutral ones are $m_1 m_2 m_N + y\lambda_1\lambda_2|H|^2 P$. The coefficient of $W\tilde{W}$ is proportional to the log of the determinant. The resultant $SW\tilde{W}$ coupling is suppressed by the ratio between $|H|^2$ and the masses of the fermions and is too small to generate the observed BAU. We may introduce mass terms $\ell\bar{L}_{1,2}$ to generate $\partial S\ell^\dagger\bar{\sigma}\ell$ coupling, which can generate the observed BAU.

6 Experimental signals

In this section, we discuss various ways to probe the ALP-assisted model.

6.1 Higgs exotic decay

The ALP-Higgs coupling leads to exotic Higgs decay, $h \to SS$. As an effective probe of scalar extensions of the SM, the Higgs exotic decay has been intensively searched at the LHC for various SM final states of S with the branching ratio determined from the mixing with the

JHEP04(2024)108

Higgs, see ref. [95] for the most updated review. High luminosity LHC (HL-LHC) and the Higgs Factory are expected to put a limit on the exotic decay branching ratio by 1-2 orders of magnitude stronger than current searches. In this model, the relevant operators up to dim-4 are $\lambda\sqrt{2}vh^3$, ASh^2, and $AS^2h\sqrt{2}v/(2f)$. The hSS coupling after the singlet-Higgs mixing is

$$g_{hSS} = 3\lambda\sqrt{2}v\sin^2\theta\cos\theta + A\sin\delta\left(\frac{3}{2}\sin^3\theta - \sin\theta\cos^2\theta\right) + \frac{A}{f}\sqrt{2}v\cos\delta\left(\frac{1}{2}\cos^3\theta - \sin^2\theta\cos\theta\right). \tag{6.1}$$

The exotic decay rate is

$$\Gamma_{hSS} = \frac{g_{hSS}^2}{32\pi m_h}\sqrt{1-4\frac{m_S^2}{m_h^2}}. \tag{6.2}$$

The effective g_{hSS} coupling has a term $Avf^{-1}\cos\delta\cos^3\theta$ where $\sin\theta$ does not appear directly. Small mixing angle θ thus suppresses this term only by making A smaller. This suppression is linear, leading to a slowly decreasing exotic branching ratio for decreasing $\sin\theta$. Though the branching ratio is beyond the reach of the current existing limit, the future Higgs exotic decay search at the Higgs factory (and HL-LHC for some specific parameter region) can probe this model further. In figure 5, we show the future projection for HL-LHC and Higgs factory for different values of c and δ. The current existing limit curves are outside the plot range.

6.2 Scalar direct production

The mixing between S and h induces interaction between S and SM gauge bosons. The vertex SZZ is used to search for S at the LEP. Searches are performed independently of the decay modes of S up to 15 GeV by the L3 Collaboration [96] and up to 100 GeV by the OPAL Collaboration [97]. Searches assuming S decaying into $b\bar{b}$ or $\tau\bar{\tau}$ is also performed up to 100 GeV [98]. In this paper, we assume that S does not decay into the dark sector and choose the most stringent bound mentioned above for each mass, leading to the purple-shaded region in figure 5. The most stringent bound comes from the decay-independent search for $m_S \lesssim 17$ GeV while from the $b\bar{b}$ final state search for larger masses. The latter can be relaxed if S dominantly decays into the dark sector.

6.3 Rare meson decay

The mixing also leads to extra decay channels of mesons such as B and K mesons. For a comprehensive review, see [99]. For the most recent updated review for experimental searches, see [100]. Here we summarize the relevant searches; the current limit and projected searches are shown in figure 5 by the shaded region and dashed line, respectively.

The B meson can decay into $K + S$ with S decaying into a muon pair. This decay chain is searched at the LHCb experiment for 200 MeV $\leq m_S \leq 4$ GeV [101, 102], constraining the mixing angle to be smaller than 10^{-3}, as shown in the upper panels in figure 5. The bound is avoided if S dominantly decays into dark-sector particles [34].

If S is lighter than the K meson, it leads to an extra decay channel $K \to \pi S$ with S further decaying into SM particles (most likely electron or muon pair if mass allowed). If m_S is

JHEP04(2024)108

smaller than $2m_\mu$, the decay rate is small and S is long-lived at the experimental scale and can thus be regarded as a stable particle, invisible final state. The NA62 experiment performed searches for long-lived, invisible S via charged kaons [103] and neutral kaons [104], respectively. E949 experiment searched for charged-kaon decay $K^+ \to \pi^+ + \text{invisible}$ [105, 106], which was reinterpreted as the bound for dark decay channel for ALPs in ref. [107]. These experiments provide strong constraints on the parameter region for this model.

Most of the currently allowed parameter space in the MeV scale can be probed by future beam-dump experiments. NA62 Run 2 is expected to finish in 2025 [100]. The proposed High Intensity Kaon Experiments (HIKE) project (also known as KLEVER), utilizing a CERN beam, is expected to perform searches at a 15-year time scale.

6.4 Heavy particles at colliders

The UV completion of the model generically predicts new particles beyond S. We expect new particles with a mass scale f in UV models for the ALP. We show the contours of $f = 1\,\text{TeV}$ by pink dashed lines in figure 5. For the GeV scale S, the contours show up in the viable parameter regions and to the right of these lines, $f < 1\,\text{TeV}$ and there may be observable collider signals from new heavy particles. For the MeV scale S, on the other hand, f varies from $10^6\,\text{GeV}$ to $10^7\,\text{GeV}$ and we do not expect signals from new particles associated with f.

We also expect particles associated with the cutoff $\Lambda_H = O(1-10)\,\text{TeV}$. In the composite/perturbative UV completion, electroweak charged NGBs/fermions with a mass around Λ_H are predicted.

6.5 Electron electric dipole moment

The electron EDM can be generated via a photon loop and has been computed in refs. [108–110].[3] Here, we consider the $SW\tilde{W}$ coupling in eq. (4.3) as an example. By matching our model parameters to refs. [108–110], we find

$$\frac{d_e}{e} = \frac{1}{64\sqrt{2}\pi^4}\frac{c_W e^2 y_e \sin\theta}{f}\ln\left(\frac{m_W}{m_S}\right) . \tag{6.3}$$

We choose c_W so that the observed BAU is explained by local electroweak baryogenesis. We show the current constraint [111] in figure 6 with dark green solid curves, above which is excluded.

For the following reasons, we only show $c = 3$ for $\delta = \pi/5, 2\pi/5$ and $c = 1.2/\sin\delta$ for $\delta = \pi/20$:

- For $\delta = 2\pi/5$, $c = 30$ case is already excluded even without the eEDM constraint, see figure 5.
- For $\delta = \pi/5$, $c = 30$ curve is very close to the $c = 3$ case.
- For $\delta = \pi/20$, $c = 1.2/\sin\delta$ and $c = 1.5/\sin\delta$ have distinguishable eEDM curves. Their exclusion curves have a similar shape, but are located at different regions. Though they

[3] A Z boson loop also contributes to the EDM. Although the products of the coupling constants in the photon and Z loops are similar, the latter does not have log-enhancement and is expected to be subdominant.

JHEP04(2024)108

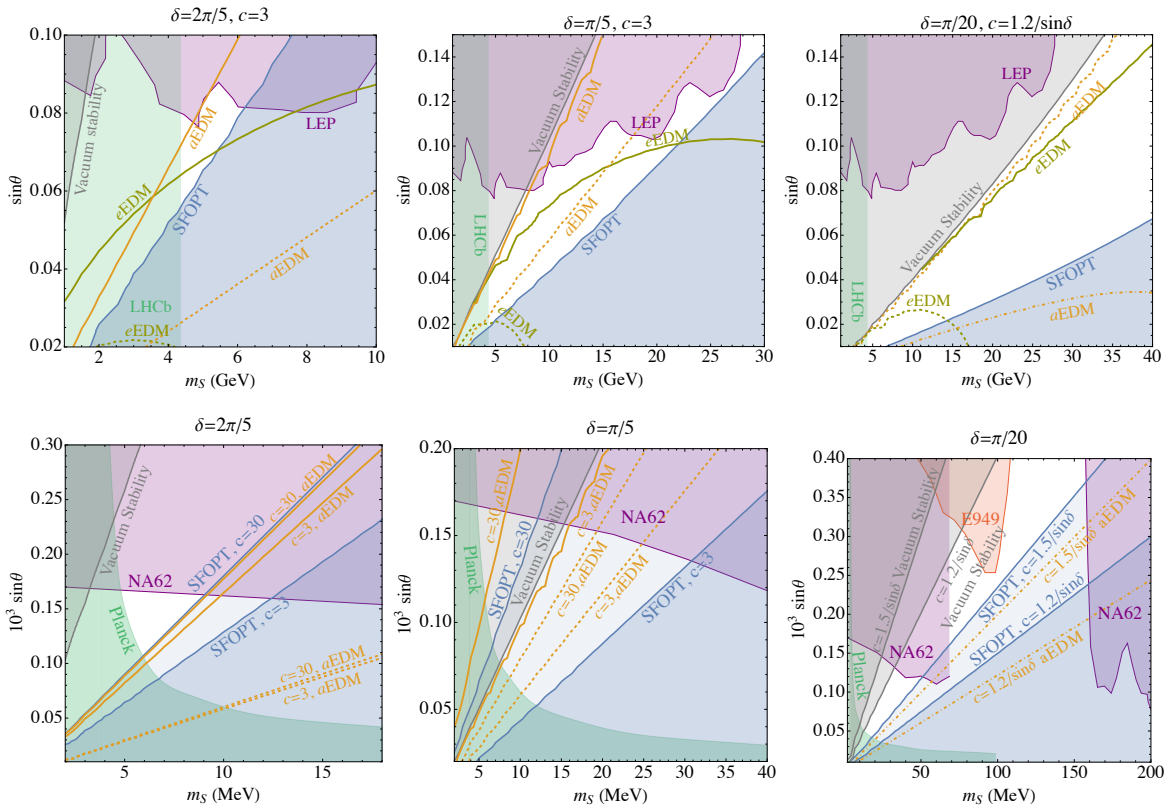

Figure 6. The EDM constraints and future prospects. The regions above the curves are excluded or will be probed. Dark green curve: electron EDM discussed in section 6.5. Orange curve: atomic EDM discussed in section 6.6. For GeV scale m_S, we only show one value of c for better visibility of the plots. Current EDM contraints are shown by solid curves while the future prospect is plotted by dashed lines for an improvement by a factor of 10 and by dot-dashed lines for a factor of 100. The improvement of the EDM constraint will fully cover the plotted range for all the panels.

prefer different parameter spaces, the total sizes of the allowed parameter space are similar to each other. For a better visibility of the plot, we choose to plot only one of them.

From the plots, one can see that the electron EDM constraint is not as severe as most of the scalar extension models. For a small mixing angle, the EDM itself is small. For a large mixing angle, the large filed value shift of S requires $c_W < 1$, and the EDM is suppressed accordingly. However, most portion of the viable parameter space of the-GeV scale m_S can still be probed in the future if the EDM reach is improved by a factor of 10 [112]; the future prospect is shown in figure 6 by dashed curves. If the improvement is by a factor of 100, then all the parameter space of the GeV scale S will be probed. The electron EDM for the MeV scale m_S, on the other hand, is more suppressed by the small mixing angle and large f, and it requires an improvement of 3-4 orders of magnitude to probe the parameter space.

The BAU may be explained by the fermionic coupling $c_\psi \partial_\mu S \psi^\dagger \bar{\sigma}^\mu \psi / f$ instead of the W coupling. There are two competing impacts on the EDM. For $c_\psi = c_W$, 1) the fermion loop generates a larger electron EDM than the photon loop, but 2) the BAU created by

JHEP04(2024)108

the fermion coupling is larger than the W coupling; see eq. (4.5). We found that the latter effect wins and the fermion model predicts a slightly smaller EDM than the W model. The qualitative conclusion for the W model holds for the fermion model.

6.6 Atomic electric dipole moment

The ALP couples to the nucleons and electrons as a CP-even scalar through the mixing with the Higgs. In the model of local electroweak baryogenesis, the ALP may couple to fermions as a CP-odd scalar. If the latter coupling exists for the electron, up quark, or down quark, the exchange of the ALP between nucleons and electrons induces atomic EDMs.

The scalar coupling is model-independently given by

$$-0.3\sin\theta\frac{m_N}{\sqrt{2}v}S\bar{N}N-\sin\theta\frac{m_e}{\sqrt{2}v}S\bar{e}e, \tag{6.4}$$

where the numerical factor of 0.3 is determined using the trace anomaly [113, 114]. The pseudo-scalar coupling is

$$-ic_\psi\frac{m_\psi}{f}S\bar{\psi}\gamma_5\psi. \tag{6.5}$$

The up-to-date constraint on the ALP-nucleon coupling from atomic EDM (aEDM) is derived in ref. [115]. In figure 6, the constraint is translated to the mixing angle and shown by solid orange curves, assuming that the coupling in eq. (6.5) exists for the electron. The coupling constant c_e is again adjusted to reproduce the observed baryon asymmetry. Parameter spaces above the curves are excluded. Similar to the electron EDM, improvement by a factor of 10 and 100 is assumed for the dashed and dotted-dashed curves. An improvement of 10 will cover most of the parameter spaces. The improvement by 100, on the other hand, will fully cover the parameter space, and the contours are below the plotted range except for the $\delta=\pi/20$ case. If the coupling in eq. (6.5) exists for the up or down quarks rather than the electron, the atomic EDM will change by an $O(1)$ factor. We note that if the coupling does not exist for the first generation of fermions, the atomic EDM is highly suppressed, but is still generated by loop-generated axion-quark or electron couplings. For example, if the ALP coupled to the W boson, the loop-generated atomic EDM will be smaller by a factor of 10^{-4} than the case with a tree-level ALP-first generation fermion couplings. An improvement of 5-6 orders of magnitude in the experiments is required to probe the viable parameter space.

6.7 Effective neutrino number

For m_S around a few MeV, S is kept in thermal equilibrium in the early universe as late as when neutrinos decouple from the thermal bath. The energy of S is transferred into photons and electrons and thus dilutes the neutrino energy density relative to photons, leading to a negative contribution to the effective neutrino number, $N_{\rm eff}$. The constraint on the parameter space and the future projection are derived in [116] using the Planck 2018 data [117] and the future CMB-S4 [118]. We show the constraint and projection with the green shaded region and dashed line in figure 5, respectively.

JHEP04(2024)108

7 Conclusion and discussion

ALPs, as pNGBs, are naturally light and weakly-interacting. In this paper, we investigated the coupling between an ALP and the Higgs to enhance the strength of EWPT and identified the viable parameter space. In comparison to the early works on this model, we performed full one-loop effective potential computation, including CW corrections and thermal resummation that can significantly reduce the strength of the EWPT. We found that the EWPT can be still of strong first order in a wide range of parameter space. The ALP can be at the MeV or GeV scale with the mixing angle with the Higgs $O(10^{-1})$ and $O(10^{-4})$ respectively. As the displacement of the field value of the ALP becomes closer to the decay constant of the ALP, the required mixing angle to achieve SFOPT becomes smaller.

We investigated the two-field phase transition dynamics. The duration of the phase transition is shorter (i.e., a larger β/H parameter) for lighter ALPs. In the viable parameter region, gravitational-wave signals are too weak to be detected.

Various ways to probe this model are discussed. For the GeV scale ALP, scalar direct production at the LEP and rare B meson decay provide stringent constraints. The allowed parameter space can be probed by Higgs exotic decay in future collider experiments. For the MeV scale ALP, existing limits come from rare kaon decay and the CMB observation of the effective neutrino number. Future CMB-S4 observation and rare kaon decay experiments can probe most of the currently allowed parameter space.

Baryon asymmetry can be produced by the coupling of the ALP with the $\mathrm{SU}(2)_L$ gauge boson or $\mathrm{SU}(2)_L$-charged fermions and the local EWBG mechanism. The observed baryon asymmetry can be produced without violating the current electron EDM bound. Future experiments can fully probe the GeV scale ALP. The MeV scale ALP can be probed if the ALP has a CP-odd coupling with the electron, up quark, or down quark.

We provided two UV completions of the model by composite dynamics or a perturbative fundamental complex scalar field. The composite one explains the smallness of the decay constant of the ALP and is consistent with the GeV scale ALP. The latter one is consistent with ALPs at both the MeV and GeV scales, but the smallness of the decay constant should be explained by further extensions of the model, such as supersymmetry, which is not necessarily at the TeV scale.

In summary, this model has a naturally light and weakly-interacting scalar that enhances the strength of EWPT, in comparison to those traditional scalar extensions whose extra singlet scalar is typically heavy and strongly interacting. Gravitational-wave signals are too weak, but instead, this ALP can be probed by the EDM, rare meson decay, CMB observation, and Higgs exotic decay, which opens up a window to probe the strong first-order electroweak phase transition.

Acknowledgments

We thank Maxim Pospelov for pointing out the constraints from atomic electric dipole moments and Philipp Schicho for providing valuable and detailed assistance when we initially tried to use the `DRalgo` package. We thank Peizhi Du, Claudius Krause, and Tong Ou for useful discussions. K.H. was partly supported by Grant-in-Aid for Scientific Research

JHEP04(2024)108

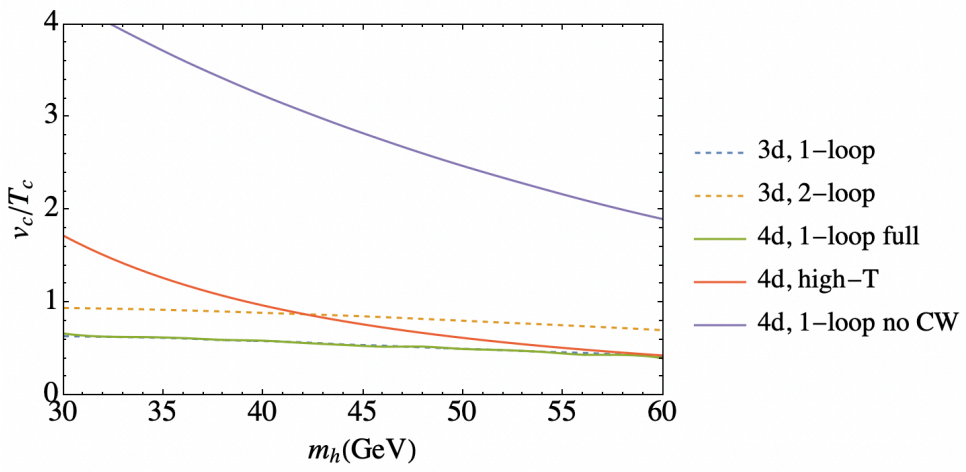

Figure 7. Comparison between different computation methods for the finite-temperature effective potential.

from the Ministry of Education, Culture, Sports, Science, and Technology (MEXT), Japan (20H01895) and by World Premier International Research Center Initiative (WPI), MEXT, Japan (Kavli IPMU). I.R.W was supported by the DOE grant DE-SC0010008. The EW-NR repository on GitLab, wrote for ref. [119], is used as a template for Python coding. The Feynman diagrams are made by the public Tikz-Feynman package [120].

A Phase transition strength in SM with lighter Higgs mass and computational uncertainties

In the introduction, we reviewed the past literature and concluded that SFOPT is unlikely to be achieved for the simplified model of eq. (1.3) in refs. [34, 37, 52]. Except for the negligible extra scalar contribution to the thermal barrier, the potential along the valley is equivalent to the SM with a small quartic coupling, i.e., a light Higgs. Here, we summarize the numerical result of the PT strength for the SM with a lighter Higgs.

Besides the computation we used in the main text, we have the following computation methods:

- Dimensional reduction with a two-loop effective potential (3d 2-loop). This computation uses the dimensional reduction method [57–60] to integrate out heavy modes and work in a 3-dimensional effective theory. It computes the effective potential up to two-loop. In addition, this computation method uses running coupling to improve the computation at finite temperatures. The input parameter is still $\overline{\text{MS}}$ renormalized under the framework of ref. [80]. This is the state-of-the-art computational method to compute the thermal effective potential.

- Dimensional reduction with a one-loop effective potential (3d 1-loop).

- Traditional one-loop computation, which is used in the main text (4d 1-loop full).

JHEP04(2024)108

- High-temperature expansion, i.e., eq. (3.4) in the SM case (4d high-T). To simplify the calculation, one widely-used way is to replace the resummation procedure by multiplying the $E_{\rm SM}$ term by a factor of 2/3 to screen out the longitudinal bosonic modes.

- Tree-level zero-temperature potential plus one-loop finite-temperature correction without resummation (4d 1-loop no CW).

We compare the result of v_c/T_c in figure 7. One can see that the 4d 1-loop no CW computation overestimates the PT strength by an $O(1)$ factor. The 4d high-T computation, although the difference is not that large, also significantly overestimate the PT strength. The 4d 1-loop full computation predicts smaller v_c/T_c and agrees with the 3d 1-loop computation. The 3d 2-loop computation predicts stronger PT, but is not yet enough to avoid the wash-out of baryon asymmetry after the EWPT. Note that the result of the 3d 2-loop computation is different from that of the 3d 1-loop computation by 50 %. This can be attributed to the cancellation of the thermal mass with the zero-temperature mass around the PT, which makes the one-loop thermal mass plus the zero-temperature mass comparable to the two-loop thermal mass [60].

Open Access. This article is distributed under the terms of the Creative Commons Attribution License (CC-BY4.0), which permits any use, distribution and reproduction in any medium, provided the original author(s) and source are credited.

References

[1] A.D. Sakharov, *Violation of CP Invariance, C asymmetry, and baryon asymmetry of the universe*, *Pisma Zh. Eksp. Teor. Fiz.* **5** (1967) 32 [INSPIRE].

[2] V.A. Kuzmin, V.A. Rubakov and M.E. Shaposhnikov, *On the Anomalous Electroweak Baryon Number Nonconservation in the Early Universe*, *Phys. Lett. B* **155** (1985) 36 [INSPIRE].

[3] G. 't Hooft, *Symmetry Breaking Through Bell-Jackiw Anomalies*, *Phys. Rev. Lett.* **37** (1976) 8 [INSPIRE].

[4] G. 't Hooft, *Computation of the Quantum Effects Due to a Four-Dimensional Pseudoparticle*, *Phys. Rev. D* **14** (1976) 3432 [*Erratum ibid.* **18** (1978) 2199] [INSPIRE].

[5] N.S. Manton, *Topology in the Weinberg-Salam Theory*, *Phys. Rev. D* **28** (1983) 2019 [INSPIRE].

[6] F.R. Klinkhamer and N.S. Manton, *A Saddle Point Solution in the Weinberg-Salam Theory*, *Phys. Rev. D* **30** (1984) 2212 [INSPIRE].

[7] N. Cabibbo, *Unitary Symmetry and Leptonic Decays*, *Phys. Rev. Lett.* **10** (1963) 531 [INSPIRE].

[8] M. Kobayashi and T. Maskawa, *CP Violation in the Renormalizable Theory of Weak Interaction*, *Prog. Theor. Phys.* **49** (1973) 652 [INSPIRE].

[9] K. Kajantie, K. Rummukainen and M.E. Shaposhnikov, *A Lattice Monte Carlo study of the hot electroweak phase transition*, *Nucl. Phys. B* **407** (1993) 356 [hep-ph/9305345] [INSPIRE].

[10] K. Farakos, K. Kajantie, K. Rummukainen and M.E. Shaposhnikov, *The electroweak phase transition at m(H) approximately = m(W)*, *Phys. Lett. B* **336** (1994) 494 [hep-ph/9405234] [INSPIRE].

JHEP04(2024)108

[11] K. Jansen, *Status of the finite temperature electroweak phase transition on the lattice*, *Nucl. Phys. B Proc. Suppl.* **47** (1996) 196 [hep-lat/9509018] [INSPIRE].

[12] K. Kajantie, M. Laine, K. Rummukainen and M.E. Shaposhnikov, *The electroweak phase transition: A Nonperturbative analysis*, *Nucl. Phys. B* **466** (1996) 189 [hep-lat/9510020] [INSPIRE].

[13] K. Rummukainen, *Finite T electroweak phase transition on the lattice*, *Nucl. Phys. B Proc. Suppl.* **53** (1997) 30 [hep-lat/9608079] [INSPIRE].

[14] K. Kajantie, M. Laine, K. Rummukainen and M.E. Shaposhnikov, *Is there a hot electroweak phase transition at $m_H \gtrsim m_W$?*, *Phys. Rev. Lett.* **77** (1996) 2887 [hep-ph/9605288] [INSPIRE].

[15] M. Gurtler, E.-M. Ilgenfritz and A. Schiller, *Where the electroweak phase transition ends*, *Phys. Rev. D* **56** (1997) 3888 [hep-lat/9704013] [INSPIRE].

[16] F. Csikor, Z. Fodor and J. Heitger, *Endpoint of the hot electroweak phase transition*, *Phys. Rev. Lett.* **82** (1999) 21 [hep-ph/9809291] [INSPIRE].

[17] M. Laine and K. Rummukainen, *A strong electroweak phase transition up to m(H) is about 105-GeV*, *Phys. Rev. Lett.* **80** (1998) 5259 [hep-ph/9804255] [INSPIRE].

[18] M. Laine and K. Rummukainen, *The MSSM electroweak phase transition on the lattice*, *Nucl. Phys. B* **535** (1998) 423 [hep-lat/9804019] [INSPIRE].

[19] K. Rummukainen et al., *The universality class of the electroweak theory*, *Nucl. Phys. B* **532** (1998) 283 [hep-lat/9805013] [INSPIRE].

[20] Z. Fodor, *Electroweak phase transitions*, *Nucl. Phys. B Proc. Suppl.* **83** (2000) 121 [hep-lat/9909162] [INSPIRE].

[21] M.B. Gavela, P. Hernandez, J. Orloff and O. Pene, *Standard model CP violation and baryon asymmetry*, *Mod. Phys. Lett. A* **9** (1994) 795 [hep-ph/9312215] [INSPIRE].

[22] P. Huet and E. Sather, *Electroweak baryogenesis and standard model CP violation*, *Phys. Rev. D* **51** (1995) 379 [hep-ph/9404302] [INSPIRE].

[23] M.B. Gavela, M. Lozano, J. Orloff and O. Pene, *Standard model CP violation and baryon asymmetry. Part 1: Zero temperature*, *Nucl. Phys. B* **430** (1994) 345 [hep-ph/9406288] [INSPIRE].

[24] M.B. Gavela et al., *Standard model CP violation and baryon asymmetry. Part 2: Finite temperature*, *Nucl. Phys. B* **430** (1994) 382 [hep-ph/9406289] [INSPIRE].

[25] M.B. Gavela, P. Hernandez, J. Orloff and O. Pene, *Standard model baryogenesis*, in the proceedings of the *29th Rencontres de Moriond: Electroweak Interactions and Unified Theories*, Meribel les Allues, France, March 12–19 (1994) [hep-ph/9407403] [INSPIRE].

[26] M. Pietroni, *The electroweak phase transition in a nonminimal supersymmetric model*, *Nucl. Phys. B* **402** (1993) 27 [hep-ph/9207227] [INSPIRE].

[27] J. Choi and R.R. Volkas, *Real Higgs singlet and the electroweak phase transition in the Standard Model*, *Phys. Lett. B* **317** (1993) 385 [hep-ph/9308234] [INSPIRE].

[28] S.W. Ham, Y.S. Jeong and S.K. Oh, *Electroweak phase transition in an extension of the standard model with a real Higgs singlet*, *J. Phys. G* **31** (2005) 857 [hep-ph/0411352] [INSPIRE].

[29] A. Noble and M. Perelstein, *Higgs self-coupling as a probe of electroweak phase transition*, *Phys. Rev. D* **78** (2008) 063518 [arXiv:0711.3018] [INSPIRE].

JHEP04(2024)108

[30] A. Ahriche, *What is the criterion for a strong first order electroweak phase transition in singlet models?*, *Phys. Rev. D* **75** (2007) 083522 [hep-ph/0701192] [INSPIRE].

[31] S. Profumo, M.J. Ramsey-Musolf and G. Shaughnessy, *Singlet Higgs phenomenology and the electroweak phase transition*, *JHEP* **08** (2007) 010 [arXiv:0705.2425] [INSPIRE].

[32] V. Barger et al., *LHC Phenomenology of an Extended Standard Model with a Real Scalar Singlet*, *Phys. Rev. D* **77** (2008) 035005 [arXiv:0706.4311] [INSPIRE].

[33] V. Barger et al., *Complex Singlet Extension of the Standard Model*, *Phys. Rev. D* **79** (2009) 015018 [arXiv:0811.0393] [INSPIRE].

[34] S. Das, P.J. Fox, A. Kumar and N. Weiner, *The Dark Side of the Electroweak Phase Transition*, *JHEP* **11** (2010) 108 [arXiv:0910.1262] [INSPIRE].

[35] A. Ashoorioon and T. Konstandin, *Strong electroweak phase transitions without collider traces*, *JHEP* **07** (2009) 086 [arXiv:0904.0353] [INSPIRE].

[36] V. Barger, D.J.H. Chung, A.J. Long and L.-T. Wang, *Strongly First Order Phase Transitions Near an Enhanced Discrete Symmetry Point*, *Phys. Lett. B* **710** (2012) 1 [arXiv:1112.5460] [INSPIRE].

[37] J.R. Espinosa, T. Konstandin and F. Riva, *Strong Electroweak Phase Transitions in the Standard Model with a Singlet*, *Nucl. Phys. B* **854** (2012) 592 [arXiv:1107.5441] [INSPIRE].

[38] D.J.H. Chung, A.J. Long and L.-T. Wang, *125 GeV Higgs boson and electroweak phase transition model classes*, *Phys. Rev. D* **87** (2013) 023509 [arXiv:1209.1819] [INSPIRE].

[39] H.H. Patel and M.J. Ramsey-Musolf, *Stepping Into Electroweak Symmetry Breaking: Phase Transitions and Higgs Phenomenology*, *Phys. Rev. D* **88** (2013) 035013 [arXiv:1212.5652] [INSPIRE].

[40] W. Huang et al., *New insights in the electroweak phase transition in the NMSSM*, *Phys. Rev. D* **91** (2015) 025006 [arXiv:1405.1152] [INSPIRE].

[41] D. Curtin, P. Meade and C.-T. Yu, *Testing Electroweak Baryogenesis with Future Colliders*, *JHEP* **11** (2014) 127 [arXiv:1409.0005] [INSPIRE].

[42] M. Jiang, L. Bian, W. Huang and J. Shu, *Impact of a complex singlet: Electroweak baryogenesis and dark matter*, *Phys. Rev. D* **93** (2016) 065032 [arXiv:1502.07574] [INSPIRE].

[43] A.V. Kotwal, M.J. Ramsey-Musolf, J.M. No and P. Winslow, *Singlet-catalyzed electroweak phase transitions in the 100 TeV frontier*, *Phys. Rev. D* **94** (2016) 035022 [arXiv:1605.06123] [INSPIRE].

[44] T. Tenkanen, K. Tuominen and V. Vaskonen, *A Strong Electroweak Phase Transition from the Inflaton Field*, *JCAP* **09** (2016) 037 [arXiv:1606.06063] [INSPIRE].

[45] C.-Y. Chen, J. Kozaczuk and I.M. Lewis, *Non-resonant Collider Signatures of a Singlet-Driven Electroweak Phase Transition*, *JHEP* **08** (2017) 096 [arXiv:1704.05844] [INSPIRE].

[46] C.-W. Chiang, M.J. Ramsey-Musolf and E. Senaha, *Standard Model with a Complex Scalar Singlet: Cosmological Implications and Theoretical Considerations*, *Phys. Rev. D* **97** (2018) 015005 [arXiv:1707.09960] [INSPIRE].

[47] G. Kurup and M. Perelstein, *Dynamics of Electroweak Phase Transition In Singlet-Scalar Extension of the Standard Model*, *Phys. Rev. D* **96** (2017) 015036 [arXiv:1704.03381] [INSPIRE].

[48] M. Carena, Z. Liu and Y. Wang, *Electroweak phase transition with spontaneous Z_2-breaking*, *JHEP* **08** (2020) 107 [arXiv:1911.10206] [INSPIRE].

JHEP04(2024)108

[49] A. Friedlander, I. Banta, J.M. Cline and D. Tucker-Smith, *Wall speed and shape in singlet-assisted strong electroweak phase transitions*, *Phys. Rev. D* **103** (2021) 055020 [arXiv:2009.14295] [INSPIRE].

[50] A. Azatov et al., *Ultra-relativistic bubbles from the simplest Higgs portal and their cosmological consequences*, *JHEP* **10** (2022) 017 [arXiv:2207.02230] [INSPIRE].

[51] K.S. Jeong, T.H. Jung and C.S. Shin, *Axionic Electroweak Baryogenesis*, *Phys. Lett. B* **790** (2019) 326 [arXiv:1806.02591] [INSPIRE].

[52] K. Harigaya and I.R. Wang, *First-Order Electroweak Phase Transition and Baryogenesis from a Naturally Light Singlet Scalar*, arXiv:2207.02867 [INSPIRE].

[53] M. Quiros, *Finite temperature field theory and phase transitions*, in the proceedings of the *ICTP Summer School in High-Energy Physics and Cosmology*, Miramare, Italy, June 29 – July 17 (1998) [hep-ph/9901312] [INSPIRE].

[54] P.B. Arnold and O. Espinosa, *The effective potential and first order phase transitions: Beyond leading-order*, *Phys. Rev. D* **47** (1993) 3546 [*Erratum ibid.* **50** (1994) 6662] [hep-ph/9212235] [INSPIRE].

[55] J. Löfgren, *Stop comparing resummation methods*, *J. Phys. G* **50** (2023) 125008 [arXiv:2301.05197] [INSPIRE].

[56] A. Ekstedt, P. Schicho and T.V.I. Tenkanen, *DRalgo: A package for effective field theory approach for thermal phase transitions*, *Comput. Phys. Commun.* **288** (2023) 108725 [arXiv:2205.08815] [INSPIRE].

[57] P.H. Ginsparg, *First Order and Second Order Phase Transitions in Gauge Theories at Finite Temperature*, *Nucl. Phys. B* **170** (1980) 388 [INSPIRE].

[58] T. Appelquist and R.D. Pisarski, *High-Temperature Yang-Mills Theories and Three-Dimensional Quantum Chromodynamics*, *Phys. Rev. D* **23** (1981) 2305 [INSPIRE].

[59] E. Braaten and A. Nieto, *Effective field theory approach to high temperature thermodynamics*, *Phys. Rev. D* **51** (1995) 6990 [hep-ph/9501375] [INSPIRE].

[60] K. Kajantie, M. Laine, K. Rummukainen and M.E. Shaposhnikov, *Generic rules for high temperature dimensional reduction and their application to the standard model*, *Nucl. Phys. B* **458** (1996) 90 [hep-ph/9508379] [INSPIRE].

[61] D. Croon et al., *Theoretical uncertainties for cosmological first-order phase transitions*, *JHEP* **04** (2021) 055 [arXiv:2009.10080] [INSPIRE].

[62] O. Gould, *Real scalar phase transitions: a nonperturbative analysis*, *JHEP* **04** (2021) 057 [arXiv:2101.05528] [INSPIRE].

[63] L. Niemi, P. Schicho and T.V.I. Tenkanen, *Singlet-assisted electroweak phase transition at two loops*, *Phys. Rev. D* **103** (2021) 115035 [arXiv:2103.07467] [INSPIRE].

[64] P.M. Schicho, T.V.I. Tenkanen and J. Österman, *Robust approach to thermal resummation: Standard Model meets a singlet*, *JHEP* **06** (2021) 130 [arXiv:2102.11145] [INSPIRE].

[65] M. Dine, P. Huet, R.L. Singleton Jr. and L. Susskind, *Creating the baryon asymmetry at the electroweak phase transition*, *Phys. Lett. B* **257** (1991) 351 [INSPIRE].

[66] M. Dine, *Electroweak baryogenesis: An Overview (where are we now?)*, in the proceedings of the *1st Yale-Texas Workshop on Baryon Number Violation at the Electroweak Scale*, New Haven, U.S.A., March 19–21 (1992) [hep-ph/9206220] [INSPIRE].

JHEP04(2024)108

[67] M. Trodden, *Electroweak baryogenesis*, *Rev. Mod. Phys.* **71** (1999) 1463 [hep-ph/9803479] [INSPIRE].

[68] J.R. Espinosa, B. Gripaios, T. Konstandin and F. Riva, *Electroweak Baryogenesis in Non-minimal Composite Higgs Models*, *JCAP* **01** (2012) 012 [arXiv:1110.2876] [INSPIRE].

[69] K.S. Jeong, T.H. Jung and C.S. Shin, *Adiabatic electroweak baryogenesis driven by an axionlike particle*, *Phys. Rev. D* **101** (2020) 035009 [arXiv:1811.03294] [INSPIRE].

[70] L. Bian, Y. Wu and K.-P. Xie, *Electroweak phase transition with composite Higgs models: calculability, gravitational waves and collider searches*, *JHEP* **12** (2019) 028 [arXiv:1909.02014] [INSPIRE].

[71] S. De Curtis, L. Delle Rose and G. Panico, *Composite Dynamics in the Early Universe*, *JHEP* **12** (2019) 149 [arXiv:1909.07894] [INSPIRE].

[72] V. Agrawal, S.M. Barr, J.F. Donoghue and D. Seckel, *Viable range of the mass scale of the standard model*, *Phys. Rev. D* **57** (1998) 5480 [hep-ph/9707380] [INSPIRE].

[73] L.J. Hall, D. Pinner and J.T. Ruderman, *The Weak Scale from BBN*, *JHEP* **12** (2014) 134 [arXiv:1409.0551] [INSPIRE].

[74] G. D'Amico, A. Strumia, A. Urbano and W. Xue, *Direct anthropic bound on the weak scale from supernovæ explosions*, *Phys. Rev. D* **100** (2019) 083013 [arXiv:1906.00986] [INSPIRE].

[75] L. Maiani, *All You Need to Know about the Higgs Boson*, *Conf. Proc. C* **7909031** (1979) 1 [INSPIRE].

[76] M.J.G. Veltman, *The Infrared - Ultraviolet Connection*, *Acta Phys. Polon. B* **12** (1981) 437 [INSPIRE].

[77] E. Witten, *Dynamical Breaking of Supersymmetry*, *Nucl. Phys. B* **188** (1981) 513 [INSPIRE].

[78] R.K. Kaul, *Gauge Hierarchy in a Supersymmetric Model*, *Phys. Lett. B* **109** (1982) 19 [INSPIRE].

[79] S.R. Coleman and E.J. Weinberg, *Radiative Corrections as the Origin of Spontaneous Symmetry Breaking*, *Phys. Rev. D* **7** (1973) 1888 [INSPIRE].

[80] D. Buttazzo et al., *Investigating the near-criticality of the Higgs boson*, *JHEP* **12** (2013) 089 [arXiv:1307.3536] [INSPIRE].

[81] A.D. Linde, *Decay of the False Vacuum at Finite Temperature*, *Nucl. Phys. B* **216** (1983) 421 [*Erratum ibid.* **223** (1983) 544] [INSPIRE].

[82] C.L. Wainwright, *CosmoTransitions: Computing Cosmological Phase Transition Temperatures and Bubble Profiles with Multiple Fields*, *Comput. Phys. Commun.* **183** (2012) 2006 [arXiv:1109.4189] [INSPIRE].

[83] G.D. Moore, *Measuring the broken phase sphaleron rate nonperturbatively*, *Phys. Rev. D* **59** (1999) 014503 [hep-ph/9805264] [INSPIRE].

[84] M. D'Onofrio, K. Rummukainen and A. Tranberg, *Sphaleron Rate in the Minimal Standard Model*, *Phys. Rev. Lett.* **113** (2014) 141602 [arXiv:1404.3565] [INSPIRE].

[85] S. Baum et al., *Nucleation is more than critical: A case study of the electroweak phase transition in the NMSSM*, *JHEP* **03** (2021) 055 [arXiv:2009.10743] [INSPIRE].

[86] V. Domcke, Y. Ema, K. Mukaida and M. Yamada, *Spontaneous Baryogenesis from Axions with Generic Couplings*, *JHEP* **08** (2020) 096 [arXiv:2006.03148] [INSPIRE].

JHEP04(2024)108

[87] R.T. Co, L.J. Hall and K. Harigaya, *Predictions for Axion Couplings from ALP Cogenesis*, *JHEP* **01** (2021) 172 [arXiv:2006.04809] [INSPIRE].

[88] J.M. Cline, K. Kainulainen and A.P. Vischer, *Dynamics of two Higgs doublet CP violation and baryogenesis at the electroweak phase transition*, *Phys. Rev. D* **54** (1996) 2451 [hep-ph/9506284] [INSPIRE].

[89] A. Manohar and H. Georgi, *Chiral Quarks and the Nonrelativistic Quark Model*, *Nucl. Phys. B* **234** (1984) 189 [INSPIRE].

[90] M.A. Luty, *Naive dimensional analysis and supersymmetry*, *Phys. Rev. D* **57** (1998) 1531 [hep-ph/9706235] [INSPIRE].

[91] A.G. Cohen, D.B. Kaplan and A.E. Nelson, *Counting 4 pis in strongly coupled supersymmetry*, *Phys. Lett. B* **412** (1997) 301 [hep-ph/9706275] [INSPIRE].

[92] R.D. Pisarski and F. Wilczek, *Remarks on the Chiral Phase Transition in Chromodynamics*, *Phys. Rev. D* **29** (1984) 338 [INSPIRE].

[93] N. Arkani-Hamed, A.G. Cohen and H. Georgi, *Electroweak symmetry breaking from dimensional deconstruction*, *Phys. Lett. B* **513** (2001) 232 [hep-ph/0105239] [INSPIRE].

[94] N. Arkani-Hamed, A.G. Cohen, E. Katz and A.E. Nelson, *The Littlest Higgs*, *JHEP* **07** (2002) 034 [hep-ph/0206021] [INSPIRE].

[95] M. Carena et al., *Probing the Electroweak Phase Transition with Exotic Higgs Decays*, *LHEP* **2023** (2023) 432 [arXiv:2203.08206] [INSPIRE].

[96] L3 collaboration, *Search for neutral Higgs boson production through the process $e^+e^- \to Z^*$ H0*, *Phys. Lett. B* **385** (1996) 454 [INSPIRE].

[97] OPAL collaboration, *Decay mode independent searches for new scalar bosons with the OPAL detector at LEP*, *Eur. Phys. J. C* **27** (2003) 311 [hep-ex/0206022] [INSPIRE].

[98] LEP Working Group for Higgs boson searches et al. collaborations, *Search for the standard model Higgs boson at LEP*, *Phys. Lett. B* **565** (2003) 61 [hep-ex/0306033] [INSPIRE].

[99] J. Beacham et al., *Physics Beyond Colliders at CERN: Beyond the Standard Model Working Group Report*, *J. Phys. G* **47** (2020) 010501 [arXiv:1901.09966] [INSPIRE].

[100] C. Antel et al., *Feebly-interacting particles: FIPs 2022 Workshop Report*, *Eur. Phys. J. C* **83** (2023) 1122 [arXiv:2305.01715] [INSPIRE].

[101] LHCb collaboration, *Search for hidden-sector bosons in $B^0 \to K^{*0}\mu^+\mu^-$ decays*, *Phys. Rev. Lett.* **115** (2015) 161802 [arXiv:1508.04094] [INSPIRE].

[102] LHCb collaboration, *Search for long-lived scalar particles in $B^+ \to K^+\chi(\mu^+\mu^-)$ decays*, *Phys. Rev. D* **95** (2017) 071101 [arXiv:1612.07818] [INSPIRE].

[103] NA62 collaboration, *Measurement of the very rare $K^+ \to \pi^+\nu\bar{\nu}$ decay*, *JHEP* **06** (2021) 093 [arXiv:2103.15389] [INSPIRE].

[104] NA62 collaboration, *Search for π^0 decays to invisible particles*, *JHEP* **02** (2021) 201 [arXiv:2010.07644] [INSPIRE].

[105] E949 collaboration, *Improved measurement of the $K^+ \to \pi^+\nu\bar{\nu}u$ branching ratio*, *Phys. Rev. Lett.* **93** (2004) 031801 [hep-ex/0403036] [INSPIRE].

[106] BNL-E949 collaboration, *Study of the decay $K^+ \to \pi^+\nu\bar{\nu}$ in the momentum region $140 < P_\pi < 199$ MeV/c*, *Phys. Rev. D* **79** (2009) 092004 [arXiv:0903.0030] [INSPIRE].

JHEP04(2024)108

[107] M.J. Dolan, F. Kahlhoefer, C. McCabe and K. Schmidt-Hoberg, *A taste of dark matter: Flavour constraints on pseudoscalar mediators*, *JHEP* **03** (2015) 171 [*Erratum ibid.* **07** (2015) 103] [arXiv:1412.5174] [INSPIRE].

[108] W.J. Marciano, A. Masiero, P. Paradisi and M. Passera, *Contributions of axionlike particles to lepton dipole moments*, *Phys. Rev. D* **94** (2016) 115033 [arXiv:1607.01022] [INSPIRE].

[109] L. Di Luzio, R. Gröber and P. Paradisi, *Hunting for CP-violating axionlike particle interactions*, *Phys. Rev. D* **104** (2021) 095027 [arXiv:2010.13760] [INSPIRE].

[110] L. Di Luzio et al., *CP-Violating Axions: A Theory Review*, arXiv:2312.17310 [INSPIRE].

[111] ACME collaboration, *Improved limit on the electric dipole moment of the electron*, *Nature* **562** (2018) 355 [INSPIRE].

[112] A.C. Vutha et al., *Search for the electric dipole moment of the electron with thorium monoxide*, *J. Phys. B* **43** (2010) 074007 [arXiv:0908.2412] [INSPIRE].

[113] M.A. Shifman, A.I. Vainshtein and V.I. Zakharov, *Remarks on Higgs Boson Interactions with Nucleons*, *Phys. Lett. B* **78** (1978) 443 [INSPIRE].

[114] R. Barbieri, L.J. Hall and K. Harigaya, *Minimal Mirror Twin Higgs*, *JHEP* **11** (2016) 172 [arXiv:1609.05589] [INSPIRE].

[115] V.A. Dzuba, V.V. Flambaum, I.B. Samsonov and Y.V. Stadnik, *New constraints on axion-mediated P,T-violating interaction from electric dipole moments of diamagnetic atoms*, *Phys. Rev. D* **98** (2018) 035048 [arXiv:1805.01234] [INSPIRE].

[116] M. Ibe, S. Kobayashi, Y. Nakayama and S. Shirai, *Cosmological constraints on dark scalar*, *JHEP* **03** (2022) 198 [arXiv:2112.11096] [INSPIRE].

[117] PLANCK collaboration, *Planck 2018 results. VI. Cosmological parameters*, *Astron. Astrophys.* **641** (2020) A6 [*Erratum ibid.* **652** (2021) C4] [arXiv:1807.06209] [INSPIRE].

[118] CMB-S4 collaboration, *CMB-S4 Science Book, First Edition*, arXiv:1610.02743 [INSPIRE].

[119] M. Carena, C. Krause, Z. Liu and Y. Wang, *New approach to electroweak symmetry nonrestoration*, *Phys. Rev. D* **104** (2021) 055016 [arXiv:2104.00638] [INSPIRE].

[120] J. Ellis, *TikZ-Feynman: Feynman diagrams with TikZ*, *Comput. Phys. Commun.* **210** (2017) 103 [arXiv:1601.05437] [INSPIRE].

JHEP04(2024)108